

1 **Observation and analysis of spatio-temporal characteristics of surface ozone and carbon**  
2 **monoxide at multiple sites in the Kathmandu Valley, Nepal**

3 Khadak Singh Mahata<sup>1,2</sup>, Maheswar Rupakheti<sup>1,3</sup>, Arnico Kumar Panday<sup>4,5</sup>, Piyush Bhardwaj<sup>6</sup>,  
4 Manish Naja<sup>6</sup>, Ashish Singh<sup>1</sup>, Andrea Mues<sup>1</sup>, Paolo Cristofanelli<sup>7</sup>, Deepak Pudasainee<sup>8</sup>, Paolo  
5 Bonasoni<sup>7</sup>, Mark G. Lawrence<sup>1,2</sup>

6

7 <sup>1</sup>Institute for Advanced Sustainability Studies (IASS), Potsdam, Germany

8 <sup>2</sup>University of Potsdam, Potsdam, Germany

9 <sup>3</sup>Himalayan Sustainability Institute (HIMSI), Kathmandu, Nepal

10 <sup>4</sup>International Centre for Integrated Mountain Development (ICIMOD), Lalitpur, Nepal

11 <sup>5</sup>University of Virginia, Charlottesville, USA

12 <sup>6</sup>Aryabhata Research Institute of Observational Sciences (ARIES), Nainital, India

13 <sup>7</sup>CNR-ISAC, National Research Council of Italy – Institute of Atmospheric Sciences and  
14 Climate, Bologna, Italy

15 <sup>8</sup>Department of Chemical and Materials Engineering, University of Alberta, Edmonton, Canada

16

17 Correspondence to: Maheswar Rupakheti ([maheswar.rupakheti@iass-potsdam.de](mailto:maheswar.rupakheti@iass-potsdam.de)) and Khadak  
18 Singh Mahata ([khadak.mahata@iass-potsdam.de](mailto:khadak.mahata@iass-potsdam.de))

19

20

21

22

23

24

25 **Abstract**

26 Residents of the Kathmandu Valley experience severe particulate and gaseous air pollution  
27 throughout most of the year, even during much of the rainy season. The knowledge base for  
28 understanding the air pollution in the Kathmandu Valley was previously very limited, but is  
29 improving rapidly due to several field measurement studies conducted in the last few years. Thus  
30 far, most analyses of observations in the Kathmandu Valley have been limited to short periods of  
31 time at single locations. This study extends the past studies by examining the spatial and  
32 temporal characteristics of two important gaseous air pollutants (CO and O<sub>3</sub>) based on  
33 simultaneous observations over a longer period at five locations within the valley and on its rim,  
34 including a supersite (at Bode in the valley center, 1345 m above sea level) and four satellite  
35 sites (at Paknajol, 1380 m asl in the Kathmandu city center, at Bhimdhunga (1522 m asl), a  
36 mountain pass on the valley's western rim, at Nagarkot (1901 m asl), another mountain pass on  
37 the eastern rim, and Naikhandi (1233 m asl), near the valley's only river outlet). CO and O<sub>3</sub>  
38 mixing ratios were monitored from January to July 2013, along with other gases and aerosol  
39 particles by instruments deployed at the Bode supersite during the international air pollution  
40 measurement campaign SusKat-ABC (Sustainable Atmosphere for the Kathmandu Valley –  
41 endorsed by the Atmospheric Brown Clouds program of UNEP). The monitoring of O<sub>3</sub> at Bode,  
42 Paknajol and Nagarkot as well as the CO monitoring at Bode were extended until March 2014 to  
43 investigate their variability over a complete annual cycle. Higher CO mixing ratios were found at  
44 Bode than at the outskirt sites (Bhimdhunga, Naikhandi and Nagarkot), and all sites except  
45 Nagarkot showed distinct diurnal cycles of CO mixing ratio with morning peaks and daytime  
46 lows. Seasonally, CO was higher during pre-monsoon (March-May) season and winter  
47 (December-February) season than during monsoon season (June-September) and post-monsoon  
48 (October-November) season. This is primarily due to the emissions from brick industries, which  
49 are only operational during this period (January-April), as well as increased domestic heating  
50 during winter, and regional forest fires and agro-residue burning during the pre-monsoon season.  
51 It was lower during the monsoon due to rainfall, which reduces open burning activities within the  
52 valley and in the surrounding regions, and thus reduces sources of CO. The meteorology of the  
53 valley also played a key role in determining the CO mixing ratios. The wind is calm and easterly  
54 in the shallow mixing layer, with a mixing layer height (MLH) of about 250 m, during the night

55 and early morning. The MLH slowly increases after the sunrises and decreases in the afternoon.  
56 As a result, the westerly wind becomes active and reduces the mixing ratio during the day time.  
57 Furthermore, there was evidence of an increase in the O<sub>3</sub> mixing ratios in the Kathmandu Valley  
58 as a result of emissions in the Indo-Gangetic Plains (IGP) region, particularly from biomass  
59 burning including agro-residue burning. A top-down estimate of the CO emission flux was made  
60 by using the CO mixing ratio and mixing layer height measured at Bode. The estimated annual  
61 CO flux at Bode was 4.9 μg m<sup>-2</sup> s<sup>-1</sup>, which is 2-14 times higher than that in widely used emission  
62 inventory databases (EDGAR HTAP, REAS and INTEX-B). This difference in CO flux between  
63 Bode and other emission databases likely arises from large uncertainties in both the top-down  
64 and bottom-up approaches to estimating the emission flux. The O<sub>3</sub> mixing ratio was found to be  
65 highest during the pre-monsoon season at all sites, while the timing of the seasonal minimum  
66 varied across the sites. The daily maximum 8 hour average O<sub>3</sub> exceeded the WHO recommended  
67 guideline of 50 ppb on more days at the hilltop station of Nagarkot (159/357 days) than at the  
68 urban valley bottom sites of Paknajol (132/354 days) and Bode (102/353 days), presumably due  
69 to the influence of free-tropospheric air at the high-altitude site, as also indicated by Putero et al.,  
70 (2015) for the Paknajol site in the Kathmandu Valley as well as to titration of O<sub>3</sub> by fresh NOx  
71 emissions near the urban sites. More than 78% of the exceedance days were during the pre-  
72 monsoon period at all sites. The high O<sub>3</sub> mixing ratio observed during the pre-monsoon period is  
73 of a concern for human health and ecosystems, including agroecosystems in the Kathmandu  
74 Valley and surrounding regions.

75

## 76 **1. Introduction**

77 Air pollution is one of the major health risks globally. It was responsible for premature loss of  
78 about 7 million lives worldwide in 2012 (WHO, 2014), with about 1.7 million of these being in  
79 South Asian countries (India, Pakistan, Nepal and Bangladesh) in 2013 (Forouzanfar, 2015). The  
80 latest report shows that the indoor and outdoor air pollution are each responsible for 4 million  
81 premature deaths every year (<http://www.who.int/airpollution/en/>). South Asia is considered to  
82 be a major air pollution hotspot (Monks et al., 2009) and it is expected to be one of the most  
83 polluted regions in the world for surface ozone (O<sub>3</sub>) and other pollutants by 2030 (Dentener et  
84 al., 2006; IEA 2016; OECD 2016). Past studies have shown that the air pollution from this

85 region affects not only the region itself, but is also transported to other parts of the world,  
86 including comparatively pristine regions such as the Himalayas and the Tibetan plateau  
87 (Bonasoni et al., 2010; Ming, et al., 2010; Lüthi et al., 2015), as well as to other distant locations  
88 such as northern Africa and the Mediterranean (Lawrence and Lelieveld, 2010). The pollutants  
89 are also uplifted to the tropopause by convective air masses and transported to the extratropical  
90 stratosphere during the monsoon season (Tissier and Legras., 2016; Lawrence and Lelieveld,  
91 2010; Fueglistaler et al., 2009; Highwood and Hoskins, 1998). Air pollution is particularly  
92 alarming in many urban areas of South Asia, including in the city of Kathmandu and the broader  
93 Kathmandu Valley, Nepal (Chen et al., 2015; Putero et al., 2015; Kim et al., 2015; Sarkar et al.,  
94 2016; Shakya et al., 2017). This is due to their rapid urbanization, economic growth and the use  
95 of poor technologies in the transportation, energy and industrial sectors. In Kathmandu  
96 topography also plays a major role: the bowl-shaped Kathmandu Valley is surrounded by tall  
97 mountains and only a handful of passes. Topography is a key factor in governing local  
98 circulations, where low MLH (typically in the range 250 m to 1,500 m) and calm winds, have  
99 been observed particularly during nights and mornings. This in turn results in poor ventilation  
100 (Mues et al., 2017). Overall, this is conducive to trapping air pollutants and the deterioration of  
101 air quality in the valley. Effectively mitigating air pollutants in the regions like the Kathmandu  
102 Valley requires scientific knowledge about characteristics and sources of the pollutants. To  
103 contribute to this urgently-needed scientific knowledge base, in this study we focus on the  
104 analysis of measurements of two important gaseous species, carbon monoxide (CO and O<sub>3</sub>, at  
105 multiple sites in and around the Kathmandu Valley. This study analyzes data from January 2013  
106 to March 2014, which includes the intensive phase of an international air pollution measurement  
107 campaign – SusKat-ABC (Sustainable Atmosphere for the Kathmandu Valley – Atmospheric  
108 Brown Clouds) – conducted during December 2012 - June 2013 (Rupakheti et al., 2018,  
109 manuscript in preparation, submission anticipated in 1-2 months), with measurements of O<sub>3</sub> and  
110 CO at some sites continuing beyond the intensive campaign period (Bhardwaj et al., 2017;  
111 Mahata et al., 2017).

112 CO is a useful tracer of urban air pollution as it is primarily released during incomplete  
113 combustion processes that are common in urban areas. Forest fires and agro-residue burning in  
114 the IGP and foothills of the Himalaya are other important contributors of CO in the region  
115 (Mahata et al., 2017; Bhardwaj et al., 2017). CO is toxic at high concentrations indoors and

116 outdoors, but our focus here is on ambient levels. The main anthropogenic sources of CO in the  
117 Kathmandu Valley are vehicles, cooking activities (using liquefied petroleum gas, kerosene, and  
118 firewood), and industries, including brick kilns, especially biomass co-fired kilns with older  
119 technologies, and until recently diesel power generator sets (Panday and Prinn, 2009; Kim et al,  
120 2015; Sarkar et al., 2016; Mahata et al., 2017; Sarkar et al., 2017). Tropospheric O<sub>3</sub>, which is  
121 formed by photochemical reactions involving oxides of nitrogen (NO<sub>x</sub>) and volatile organic  
122 compounds (VOCs), is a strong oxidizing agent in the troposphere. Because of its oxidizing  
123 nature, it is also deleterious to human health and plants already at typically polluted ambient  
124 levels (Lim et al., 2012; Burney and Ramanathan, 2014; Feng, 2015; Monks et al., 2015).  
125 Tropospheric O<sub>3</sub> is estimated to be responsible for about 5-20 % of premature deaths caused by  
126 air pollution globally (Brauer et al., 2012; Lim et al., 2012; Silva et al., 2013). It has also been  
127 estimated that high concentrations of O<sub>3</sub> are responsible for a global loss of crops equivalent to \$  
128 11-18 billion annually (Avnery et al., 2011; UNEP and WMO, 2011), a substantial fraction of  
129 which is associated with the loss in wheat in India alone (equivalent to \$ 5 billion in 2010)  
130 (Burney and Ramanathan, 2014). O<sub>3</sub> can also serve as a good indicator of the timing of the  
131 breakup of the nighttime stable boundary layer (when the ozone levels increase rapidly in the  
132 morning due to downward transport from the free troposphere (Panday and Prinn, 2009; Geiß et  
133 al., 2017).

134 Only a few past studies have reported measurements of ambient CO mixing ratios in the  
135 Kathmandu Valley. Davidson et al. (1986) measured CO in the city center and found mixing  
136 ratios between 1 and 2.5 ppm in the winter (December – February) of 1982-1983. Panday and  
137 Prinn (2009) measured similar levels of CO mixing ratios during September 2004 – June 2005,  
138 although the main sources of CO shifted from biofuel-dominated air pollutants from cooking  
139 activities in the 1980s to vehicle-dominated pollutants in the 2000s. The growth rate in the  
140 vehicle fleet has had a substantial influence on air pollution in the valley, including CO and O<sub>3</sub>.  
141 Out of 2.33 million vehicles in Nepal, close to half of them are in the Kathmandu Valley (DoTM,  
142 2015). Shrestha et al. (2013) estimated annual emission of CO of 31 kt in 2010 from a fraction  
143 of today's vehicle fleet in the Kathmandu Valley by using data from a field survey as input to the  
144 International Vehicle Emission (IVE) model. The model simulation considered motorcycles,  
145 buses, taxis, vans and three wheelers, but did not include personal cars, trucks and non-road

146 vehicles. The studied fleets covered ~73% of the total fleet (570,145) registered in the valley in  
147 2010, with motorcycles being the most common vehicle (69% of the total fleet).

148 Past studies have investigated the diurnal and seasonal variations of CO and O<sub>3</sub> mixing ratios in  
149 the Kathmandu Valley. Panday and Prinn (2009) observed distinct diurnal variations of CO  
150 mixing ratios and particulate matter concentrations observed during September 2004 – June 2005  
151 at Bouddha (about 4 km northwest of the SusKat-ABC supersite at Bode), with morning and  
152 evening peaks. They found for the Kathmandu Valley that such peaks were created by the  
153 interplay between the ventilation, as determined by the local meteorology, and the timing of  
154 emissions, especially traffic and cooking emissions. The morning CO peak was also associated  
155 with the recirculation of the pollutants transported down from an elevated residual pollution  
156 layer (Panday and Prinn, 2009).

157 O<sub>3</sub> was observed to have lower nighttime levels in the city center than at the nearby hilltop site of  
158 Nagarkot (Panday and Prinn, 2009). Pudasainee et al. (2006) studied the seasonal variations of  
159 O<sub>3</sub> mixing ratios based on the observation for a whole year (2003-2004) in Pulchowk in the  
160 Lalitpur district, just south of central Kathmandu Metropolitan City (KMC) in the Kathmandu  
161 Valley. They reported seasonal O<sub>3</sub> mixing ratios to be highest during the pre-monsoon (March –  
162 May) and lowest in the winter (December – February). As a part of the SusKat-ABC Campaign,  
163 Putero et al. (2015) monitored O<sub>3</sub> mixing ratios at Paknajol, an urban site in the center of the  
164 KMC over a full-year period (February 2013-January 2014). They also observed similar seasonal  
165 variations in O<sub>3</sub> mixing ratios in the valley to those observed by Pudasainee et al. (2006), with  
166 highest O<sub>3</sub> during the pre-monsoon (1 February – 12 May) season, followed by the monsoon (13  
167 May – 6 October), post-monsoon (7 October – 26 October) and winter (27 October – 31 January)  
168 seasons. They found that during the pre-monsoon season, westerly winds and regional synoptic  
169 circulation transport O<sub>3</sub> and its precursors from regional forest fires located outside the  
170 Kathmandu Valley. In another study conducted as part of the SusKat-ABC Campaign, 37 non-  
171 methane volatile organic compounds (NMVOCs) were measured at Bode, with data recording  
172 every second, during winter of 2012-2013; the measurements included isoprene, an important  
173 biogenic precursor of O<sub>3</sub> (Sarkar et al., 2016). They found concentrations to vary in two distinct  
174 periods. The first period was marked by no brick kiln operations and was associated with high  
175 biogenic emissions of isoprene. During the second period nearby brick kilns, which use coal

176 mixed with biomass, were in; they contributed to elevated concentrations of ambient acetonitrile,  
177 benzene and isocyanic acid. Furthermore, the authors found that oxygenated NMVOCs and  
178 isoprene combined accounted for 72% and 68% of the total O<sub>3</sub> production potential in the first  
179 period and second period, respectively.

180 Prior to the SusKat-ABC campaign there were no studies that simultaneously measured ambient  
181 CO and O<sub>3</sub> mixing ratios at multiple sites in the Kathmandu Valley over extended periods of  
182 time. Past studies either focused on one long-term site, or on short-term observation records at  
183 various sites (Panday and Prinn, 2009), or they investigated the seasonal characteristics of single  
184 pollutants such as O<sub>3</sub> at a single site in the valley (Pudasainee et al., 2006). The most comparable  
185 past study is by Putero et al. (2015), who described O<sub>3</sub> mixing ratios at one SusKat-ABC site  
186 (Paknajol) in the Kathmandu city center observed during the SusKat-ABC campaign, and  
187 discussed O<sub>3</sub> seasonal variations. There is also a companion study on regional CO and O<sub>3</sub>  
188 pollution by Bhardwaj et al. (2017) which is based on O<sub>3</sub> and CO mixing ratios monitored at the  
189 SusKat-ABC supersite at Bode in the Kathmandu Valley for a limited period (January-June  
190 2013) and at two sites in India (Pantnagar in Indo-Gangetic Plain and Nainital in Himalayan  
191 foothill). They reported simultaneous enhancement in O<sub>3</sub> and CO levels at these three sites in  
192 spring, highlighting contribution of regional emissions, such as biomass burning in northwest  
193 Indo-Gangetic Plain (IGP), and regional transport to broader regional scale pollution, including  
194 in the Kathmandu Valley. In this study, we document the diurnal and seasonal (where applicable)  
195 characteristics and spatial distributions of CO and O<sub>3</sub> mixing ratios based on simultaneous  
196 observations at several locations within the valley and on the valley rim mountains over a full  
197 year, helping to characterize the pollution within the valley and the pollution plume entering and  
198 exiting the valley. We also compute the first top-down estimates of CO emission fluxes for the  
199 Kathmandu Valley and compare these to CO emissions fluxes in widely-used emission datasets  
200 such as EDGAR HTAP (Janssens-Maenhout et al., 2000), REAS (Kurokawa et al., 2013) and  
201 INTEX-B (Zhang et al., 2009).

202

## 203 **2. Study sites and methods**

204 The Kathmandu Valley, situated in the foothills of the Central Himalaya, is home to more than 3  
205 million people. The valley floor has an area of about 340 km<sup>2</sup>, with an average altitude of about  
206 1300 m above sea level (m asl). It is surrounded by peaks of about 1900-2800 m asl. The valley

207 has five major mountain passes on its rim: the Nagdhunga, Bhimdhunga and Mudku Bhanjhyang  
208 passes in the west, and the Nala and Nagarkot passes in the east, as shown in Figure 1. The  
209 passes are situated at altitudes of 1480-1530 m asl. There is also one river outlet (the Bagmati  
210 River) towards the south, which constitutes a sixth pass for air circulation in and out of the valley  
211 (Regmi et al., 2003; Panday and Prinn, 2009). We selected five measurement sites, including two  
212 on the valley floor (Bode and Paknajol), two on mountain ridges (Bhimdhunga and Nagarkot)  
213 and one near the Bagmati River outlet (Naikhandi) to characterize the spatial and temporal  
214 variabilities of CO and O<sub>3</sub> mixing ratios in the Kathmandu Valley. A short description of the  
215 measurement sites is presented here and in Table 1, while details on instruments deployed at  
216 those sites for this study are presented in Table 2. Further details of the measurement sites are  
217 described in the SusKat-ABC campaign overview paper (Rupakheti et al., 2017, manuscript in  
218 preparation).

219  
220 Bode (27.69°N and 85.40°E, 1344 m asl): This was the supersite of the SusKat-ABC Campaign.  
221 Bode is located in the Madhyapur Thimi municipality in the just east of the geographic center of  
222 the valley. It is a semi-urban site surrounded by urban buildings and residential houses scattered  
223 across agricultural lands. Within 4 km there are 10 brick kilns and the Bhaktapur Industrial  
224 Estate towards the southeast (refer to Sarkar et al., 2016; Mahata et al., 2017 for details). The O<sub>3</sub>  
225 and CO instruments at Bode site were placed on the fifth floor of a 6-story building, the tallest in  
226 the area. The inlets of the CO and O<sub>3</sub> analyzers were mounted on the roof top of the temporary  
227 lab, 20 m above the ground level.

228  
229 Bhimdhunga: This site (27.73°N, 85.23°E, 1522 m asl) is located on the Bhimdhunga pass on the  
230 western rim of the valley. It is one of the lowest points on the north-south running mountain  
231 ridge between the Kathmandu Valley to the east and a valley of a tributary of the Trishuli River  
232 to the west. It is situated about 5.5 km from the western edge of the KMC (Kathmandu  
233 Metropolitan City), in a rural setting with very few scattered rural houses nearby. The CO  
234 instrument was placed on the ground floor of a small one-story building and its inlet was 2 m  
235 above ground. An automatic weather station (AWS) (Hobo Onset, USA) was set up on the roof  
236 of another one-story building at a distance of ca. 15 m from the first building.

237

238 Paknajol: This site (27.72°N, 85.30°E, 1380 m asl) is located at the city center in the KMC, near  
239 the popular touristic area of Thamel. It is in the western part of the valley and about 10 km  
240 distance from the Bode supersite. The O<sub>3</sub> and meteorological instruments relevant to this study  
241 were placed on the top floor and rooftop of a 6-story building, the tallest in the area (details in  
242 Putero et al., 2015; note that CO was not measured here). The inlet of the O<sub>3</sub> analyzer was placed  
243 25 m above the ground.

244  
245 Naikhandi: This site (27.60°N, 85.29°E, 1233 m asl) is located within the premises of a school  
246 (Kamdheni Madhyamik Vidhyalaya) located at the southwestern part of the valley (~7 km south  
247 from the nearest point of the Ring Road). The school premise is open, surrounded by sparsely  
248 scattered rural houses in agricultural lands. The nearest village (~75 houses) is about 500 m away  
249 in the southwest direction. There are 5 brick kilns within 2 km distance (2 to the north and 3 to  
250 the northeast) from the site. The instruments were kept in a one-story building of the school and  
251 its inlet was 5 m above the ground. The AWS (Hobo Onset, USA) was installed on the ground  
252 near the Bagmati River, ~100 m away from the main measurement site.

253  
254 Nagarkot: This site is located on a mountain ridge (27.72°N, 85.52°E, 1901 m asl), ca. 13 km  
255 east of Bode, in the eastern part of the valley. The site faces the Kathmandu Valley to the west  
256 and small rural town, Nagarkot, to the east. The instruments were set up in a 2-story building of  
257 the Nagarkot Health Post and their inlets were 5 m above the ground. The AWS (Vaisala  
258 WXT520, Finland) was set up on the roof of the building.

259  
260 Bhimdhunga Pass in the west and Naikhandi near the Bagmati River outlet in the southwest are  
261 the important places for interchange of valley air with outside air. The Bhimdhunga and  
262 Naikhandi sites are approximately 5.5 and 7 km away from the nearest edge of the city,  
263 respectively. Similarly, Bode is located downwind of the city centers and thus receives pollution  
264 outflow from nearby city centers of Kathmandu/Lalitpur due to strong westerly and  
265 southwesterly winds (4-6 m s<sup>-1</sup>) during the day time, and emissions from the Bhaktapur area to  
266 the east and southeast direction by calm easterly winds (< 1 m s<sup>-1</sup>) during the night (Sarkar et al.,  
267 2016; Mahata et al., 2017).

268

269 A freshly calibrated new CO analyzer (Horiba APMA-370, Japan) was deployed for the first  
270 time at Bode. This instrument is based on the IR absorption method at 4.6  $\mu\text{m}$  by CO molecules.  
271 Before field deployment at Bode, it was compared with the bench model of the Horiba (APMA-  
272 370), and the correlation ( $r$ ) between them was 0.9 and slope was 1.09. The instrument was  
273 regularly maintained by running auto-zero checks (Bhardwaj et al., 2017). Similarly, another CO  
274 analyzer (Picarro G2401, USA) which is based on cavity ring-down spectroscopy technique  
275 (CRDS) was also a new factory calibrated unit, and was deployed in Bode along with the Horiba  
276 APMA-370. An IR-based Thermo CO monitor (model 48i-TLE) was run simultaneously with a  
277 co-located cavity ring down spectrometry based Picarro CO analyzer for nearly 3 months. The  
278 correlation coefficient and slope between the two measurements were found to be 0.99 and 0.96,  
279 respectively (Mahata et al., 2017). This indicates that there was very little drift in the IR-based  
280 CO values due to room temperature change, within acceptable range (i.e., within the  
281 measurement uncertainties of the instruments). Therefore, we did not any apply correction in the  
282 IR-based CO data. All other CO analyzers (Thermo Scientific, 48i-TLE, USA), which are also  
283 based on IR absorption by CO molecules, deployed at Bhimdhunga, Naikhandi and Nagarkot,  
284 were set up for regular automatic zero checks on a daily basis. In addition, a span check was also  
285 performed during the observations by using span gas of 1.99 ppm (Gts-Welco, PA, USA) on  
286 March 8, 2013 at Naikhandi and Nagarkot, and on March 9 at Bhimdhunga. The IR-based CO  
287 instruments' span drifts were within a 5 % range.

288  
289 For the O<sub>3</sub> monitor (Teledyne 400E, USA) at Bode, regular zero and span checks were carried  
290 out using the built-in O<sub>3</sub> generator and scrubber (Bhardwaj et al., 2017). This unit was used in  
291 Bode from 01 January 2013 to 09 June 2013. New factory-calibrated O<sub>3</sub> monitors (Thermo  
292 Scientific, 49i, USA) were used for the rest of the measurement period (18 June 2013 to 31  
293 December 2013) at Bode, and for the full year of measurements at Nagarkot. A Thermo  
294 Environmental O<sub>3</sub> analyzer (Model 49i, USA) was used at the Paknajol site (Putero et al., 2015)  
295 with the same experimental set up as described in Cristofanelli et al. (2010). The working  
296 principle of all of the O<sub>3</sub> instruments is based on the attenuation of UV radiation by O<sub>3</sub> molecules  
297 at ~254 nm.

298 In order to characterize observations across the seasons, we considered the following seasons as  
299 defined in Shrestha et al. (1999) and used in other previous studies in the Kathmandu Valley

300 (Sharma et al., 2012; Chen et al., 2016; Mahata et al, 2017): Pre-monsoon (March, April, May);  
301 Monsoon (June, July, August September); Post-monsoon (October, November); and Winter  
302 (December, January, February).

303

### 304 **3. Results and discussion**

#### 305 **3.1 CO mixing ratio at multiple sites**

306 Figure 2 shows the time series of the hourly average CO mixing ratios at the four sites (Bode,  
307 Bhimdhunga, Naikhandi and Nagarkot). Fluctuations in CO mixing ratios were higher during the  
308 winter and pre-monsoon than during the monsoon season at all sites. The monsoon rain generally  
309 starts in Nepal around mid-June. In 2013, however, there were more frequent rain events in the  
310 month of May than in previous years. The CO mixing ratios (measured in parts per billion by  
311 volume, hereafter the unit is denoted as ppb) of hourly averaged data over the total observation  
312 periods at four sites and their standard deviation were: Bode ( $569.9 \pm 383.5$ ) ppb during 1  
313 January - 15 July, Bhimdhunga ( $321.5 \pm 166.2$ ) ppb during 14 Jan - 15 July, Naikhandi ( $345.4 \pm$   
314  $147.9$ ) ppb during 3 January - 6 June and Nagarkot ( $235.5 \pm 106.2$ ) ppb during 13 February - 15  
315 July (except 4 April to 7 June). Nagarkot had only about 3 months of CO data (due to a problem  
316 in zeroing of the instrument) during the observation period. For the measurement period, the CO  
317 mixing ratio at Nagarkot (~13 km far from Bode) showed small fluctuations compared with the  
318 other sites. High CO values in the Kathmandu Valley during the dry season (November-May)  
319 were also reported by Panday and Prinn (2009) based on their measurements during September  
320 2004-May 2005 at Bouddha (~ 4 km in northwest from Bode). The simultaneous episodes of  
321 high CO observed from April 1 to 15 in Bhimdhunga, Bode and Naikhandi indicate the influence  
322 of regional sources, in addition to local sources. This is discussed further in section 3.2.3.

323

#### 324 **3.2 Diurnal and seasonal variations of CO**

##### 325 **3.2.1 Diurnal pattern of CO at multiple sites**

326 Figure 3 shows the diurnal cycles of CO mixing ratios at four sites (plotted for the period of 13  
327 February to 3 April 2013, when the data were available from all four sites). The variation in the  
328 mixing ratios during the day was characterized by a pronounced morning peak, a weaker evening  
329 peak, and a daytime low; except at Nagarkot where peaks are less visible. Multiple sources

330 contribute to the morning and evening peaks, especially emission from vehicles, residential  
331 burning (fossil fuel and biomass), brick kilns and trash burning (Kim et al., 2015; Sarkar et al.,  
332 2016; Mahata et al., 2017). Other studies conducted during the SusKat-ABC campaign have  
333 identified garbage (household waste and yard waste) burning as a key source of various air  
334 pollutants, such as OC and EC (Kim et al., 2015), PAHs (Chen et al., 2015), and NMVOCs  
335 (Sarkar et al., 2016; Sarkar et al., 2017). Garbage burning is often done in small fires and quite  
336 sporadic, normally taking place in the evenings and mornings (partly chosen to avoid attention  
337 from the responsible authorities). The rate of waste (and also biomass) burning in the morning is  
338 higher in winter due to the use of the fires for providing warmth on colder days.

339 The observed diurnal cycle of CO is similar to that reported in a previous study (Panday and  
340 Prinn, 2009), and is also similar to the diurnal pattern of black carbon (BC) in the Kathmandu  
341 Valley (Sharma et al., 2012; Mues et al., 2017). The diurnal cycles of these primary pollutants  
342 are closely coupled with the valley's boundary layer height, which is about 1200 m during  
343 daytime, and falls to approximately 200 m at nighttime in Bode (Mues et al., 2017). Nagarkot  
344 and Bhimdhunga, both on mountain ridges, are generally above the valley's boundary layer,  
345 especially at night, and thus the diurnal profile especially at Nagarkot is distinct compared to  
346 other three sites, being relatively flat with small dip during 12:00-18:00.

347  
348 Distinct morning peaks were observed in Bode, Bhimdhunga and Naikhandi at 08:00, 09:00, and  
349 10:00, respectively, i.e., the morning peak lags by 1-2 hours in Bhimdhunga and Naikhandi  
350 compared to Bode. Bhimdhunga on the mountain ridge may receive the Kathmandu Valley's  
351 pollution due to upslope winds ( $\sim 2 \text{ m s}^{-1}$ ) from the east direction in the morning hours after the  
352 dissolution of the valley's boundary layer due to radiative heating of the mountain slopes. On the  
353 other hand, Naikhandi is in close proximity to brick kilns and could be impacted by their plumes  
354 carried to the site by northerly winds in the early morning (ca. 07:00-10:00, not shown). The  
355 evening peak values at Bode and Bhimdhunga were less pronounced compared to the morning  
356 maxima. The morning peak at Bode was influenced by nighttime accumulation of CO along with  
357 other pollutants from nearby brick kilns (Sarkar et al., 2016; Mahata et al., 2017; Mues et al.,  
358 2017) and recirculation of air from above (Panday and Prinn, 2009). Similarly, the local  
359 pollution from the nearby village and city area due to upslope winds from the valley floor is  
360 expected to contribute to the morning peak at Bhimdhunga. The evening peak at Naikhandi was

361 at 21:00 and was closer to the morning values in comparison to the large difference between  
362 morning and evening peaks at Bode and Bhimdhunga. A nighttime build-up (linear increase) of  
363 various pollutants compared to the afternoon minimum was typically observed in Bode during  
364 the SusKat-ABC measurement period, including the main campaign period (Sarkar et al., 2016;  
365 Mahata et al., 2017; Mues et al., 2017). This is mainly associated with the persistent emissions  
366 such as those from brick kilns, which are in close proximity to the Bode measurement site under  
367 the stable boundary layer. The isolated peak during the morning transition phase at Bhimdhunga  
368 could be due to an elevated polluted layer because of the slope wind (Panday et al., 2009). There  
369 appears to be less influence of nighttime polluting sources at Naikhandi and Bhimdhunga than at  
370 Bode.

371  
372 The MLH starts increasing after radiative heating of the surface by incoming solar radiation. The  
373 heating of the ground causes thermals to rise from the surface layer resulting in the entrainment  
374 of cleaner air from above the boundary layer leading to the dissolution of nocturnal stable  
375 boundary layer. Increasing wind speeds ( $4-6 \text{ m s}^{-1}$ ) during daytime also support turbulent vertical  
376 diffusion, as well as flushing of the pollution by less polluted air masses from outside the valley,  
377 with stronger horizontal winds allowing significant transport of air masses into the valley. In  
378 addition, reduced traffic and household cooking activities during daytime compared to morning  
379 and evening rush hours contribute to the reduced CO mixing ratios.

380

### 381 **3.2.2 CO diurnal variation across seasons**

382 Due to the lack of availability of simultaneous CO data at all sites covering the entire sampling  
383 period, a one-month period was selected for each season to examine the diurnal variation across  
384 the seasons, and to get more insights into the mixing ratios at different times of the day, as  
385 reported in Table 4. Figure 4 shows the diurnal variation of CO mixing ratios in Bode,  
386 Bhimdhunga, and Naikhandi during the selected periods for the three seasons.

387

388 The diurnal cycles during each season had different characteristics. The most prominent  
389 distinction was that the CO mixing ratio was low during the monsoon period over all sites  
390 (Figure 4, Table 4) as a result of summer monsoon rainfall in the valley, which is 60 - 90% of the  
391 1400 mm rainfall for a typical year (Nayava, 1980; Giri et al., 2006). Because of the rainfall, the

392 brick production activities are stopped in the valley (usually they are operational from January-  
393 April every year). Further, the rainfall also diminishes many burning activities (forest fires, agro-  
394 residue and trash burning) within the valley and surrounding region, and thus reduces CO  
395 emissions. Afternoon CO mixing ratios were higher in the pre-monsoon season than in the other  
396 two seasons in Bode, Bhimdhunga and Naikhandi (also see Table 4), with the most likely  
397 sources being emissions from forest fires and agro-residue burning arriving from outside the  
398 valley during this season (this will be discussed further in section 3.2.3). Nighttime accumulation  
399 was observed in Bode and Bhimdhunga, but not at Naikhandi, where the mixing ratio decreased  
400 slightly from about 20:00 until about 04:00, after which the mixing ratios increased until the  
401 morning peak. The nighttime accumulation of CO in Bode during pre-monsoon and winter is due  
402 to the influence of nearby brick kilns (Mahata et al., 2017) because of the calm easterly wind  
403 (refer supplementary Figure S2 in Mahata et al., 2017). Previous studies carried out at the Bode  
404 site during the SusKat-ABC campaign have attributed over a dozen brick kilns located near Bode  
405 as strong sources of BC and EC (Kim et al., 2015; Mues et al., 2017), NMVOCs (Sarkar et al.,  
406 2016; Sarkar et al., 2017), SO<sub>2</sub> (Kiros et al., 2016) and CO (Mahata et al., 2017), and the  
407 enhanced concentrations were observed during nighttime and mornings when winds blew from  
408 east and southeast bringing emissions from the location of the brick kilns to the observation site.

409  
410 Bhimdhunga is not near any major polluting sources such as brick kilns, and it is unclear whether  
411 the nighttime CO accumulation in Bhimdhunga is primarily due to ongoing local residential  
412 pollution emissions, and/or to pollution transported from remote sources. The transition of the  
413 wind from westerlies during the day to easterlies during the night, with moderate wind speed  
414 ( $\sim 2-4 \text{ m s}^{-1}$ ) at Bhimdhunga, may bring polluted air masses westwards which were initially  
415 transported to the eastern part from the Kathmandu Valley during the daytime (Regmi et al.,  
416 2003; Panday and Prinn, 2009; Panday et al., 2009).

417 The distinct shift in the morning peak was seen at all 3 sites by season. The one hour shift in the  
418 morning peak from the pre-monsoon to winter is due to an earlier onset of the morning  
419 transition. However, the one hour difference in the morning peak between Bode (pre-monsoon at  
420 8:00; winter at 9:00) and Bhimdhunga/Naikhandi (pre-monsoon at 9:00; winter at 10:00) in the  
421 pre-monsoon and winter is associated with commencement of early local emissions under the

422 shallow boundary layer at Bode. The one hour lag in the morning peak at Bhimdhunga and  
423 Naikhandi may be due to transport of city pollutants to the site, respectively.

424 Across the seasons, the afternoon (12:00-16:00) CO mixing ratio was higher during the pre-  
425 monsoon than in the winter at all three stations ( $p$  value for all sites  $< 0.5$ ) (Table 4), although the  
426 mixing layer was higher in the pre-monsoon season than in the winter in Bode (and presumably  
427 at the other sites as well). This is not likely to be explained by local emissions in the valley, since  
428 these are similar in the winter and pre-monsoon periods. Putero et al. (2015) suggested instead  
429 that this reflects an influx of polluted air into the valley due to large synoptic circulation patterns  
430 during the pre-monsoon season. Such regional influences are explored further in the next section.  
431

### 432 **3.2.3 Regional influence on CO in the valley**

433 Recent studies have indicated the likelihood of regional long-range transport contributing to air  
434 pollution in different parts of Nepal (Marinoni et al., 2013; Tripathee et al., 2014; Dhungel et al.,  
435 2016; Rupakheti et al., 2016; Lüthi et al., 2016; Wan et al., 2017), including the Kathmandu  
436 Valley, especially during the pre-monsoon period (Panday and Prinn, 2009; Putero et al., 2015;  
437 Bhardwaj et al., 2017). During the pre-monsoon season, frequent agro-residue burning and forest  
438 fires are reported in the IGP region including southern Nepal and the Himalayan foothills in  
439 India and Nepal (Ram and Sarin, 2010; Vadrevu et al., 2012), and in the Kathmandu Valley. This  
440 season is also characterized by the strongest daytime local wind speeds (averaging  $4-6 \text{ m s}^{-1}$ ) in  
441 the Kathmandu Valley (Mahata et al., 2017). Our study also observed several episodes of days  
442 with both elevated CO mixing ratios (Figure 2) and  $\text{O}_3$  mixing ratios (also measured in parts per  
443 billion by volume, hereafter the unit is denoted as ppb) (Figure 5) during April and May,  
444 especially during the late afternoon period. The influence of regional pollutants was investigated  
445 by comparing a 2-week period with normal CO levels (16–30 March (hereafter “period I”) with  
446 an adjacent two week period (1-15 April) with episodically high CO mixing ratios (hereafter  
447 “period II”), which nicely fit with the “burst” in regional fire activity presented by Putero et al.  
448 (2015) in their Figure 9. The t-test of the two hourly data means of CO in period I and period II  
449 at Bode, Bhimdhunga and Naikhandi (as in Figure 5) were performed at 95% confidence level  
450 and the differences were found to be statistically significant ( $p < 0.5$ ).

451 Figure 5a shows the diurnal cycle of CO mixing ratios during period I (faint color) and period II  
452 (dark color) at Bode, Bhimdhunga and Naikhandi. The difference between two periods was  
453 calculated by subtracting the average of period I from average of period II. The average CO  
454 mixing ratios during period II were elevated with respect to period I by 157 ppb at Bode, 175  
455 ppb at Bhimdhunga, and 176 ppb at Naikhandi. The enhancements in mixing ratios at the three  
456 sites were fairly similar from hour to hour throughout the day, with the exception of the late  
457 afternoon when the enhancement was generally greatest. This consistency across the sites  
458 suggests that the episode was caused by a large-scale enhancement (regional contribution) being  
459 added onto the prevailing local pollution levels at all the sites. A large-scale source would also  
460 be consistent with the greater enhancements of CO at the outskirt sites, which would be most  
461 directly affected by regional pollution, compared to the central valley site of Bode, with strong  
462 local sources. The enhancement during the period II is substantial (statistically significant as  
463 mentioned above), representing an increase of approximately 45% at the outskirt sites of  
464 Bhimdhunga and Naikhandi (which start with lower CO levels), and 23% at Bode. During both  
465 periods I and II, local winds from west (the opposite direction from the brick kilns, which were  
466 mostly located to the southeast of Bode) were dominant during daytime at Bode (Figure 5b, c).  
467 This suggests that the elevation in CO levels was caused by additional emissions in period II in  
468 the regions to the west and southwest of the Kathmandu Valley, e.g., large scale agricultural  
469 burning and forest fires during this period, as also noted by Putero et al. (2015) (see their Figure  
470 9). Far away, in Lumbini in the southern part of Nepal (Rupakheti et al., 2016), and Pantnagar in  
471 northern IGP in India (Bharwdwaj et al., 2017), about 220 km (aerial distance) to the southwest  
472 and 585 km to the west, respectively, of the Kathmandu Valley, CO episodes were also observed  
473 during the spring season of 2013, providing a strong indication that the episode in period II was  
474 indeed regional in nature.

475

### 476 **3.3 O<sub>3</sub> in the Kathmandu Valley and surrounding areas**

477 Figure 6 shows the hourly average and daily maximum 8-hour average of O<sub>3</sub> mixing ratios at  
478 Bode, Paknajol, and Nagarkot from measurements during the SusKat campaign and afterwards,  
479 along with O<sub>3</sub> mixing ratios from a previous study (November 2003 - October 2004; Pudasainee  
480 et al., 2006) at the Pulchowk site (4 km away from Paknajol) in the Latitpur district. The daily  
481 maximum 8-hour average O<sub>3</sub> was calculated by selecting the maximum O<sub>3</sub> mixing ratio from 8

482 hour running averages during each day. The nighttime mixing ratio of hourly O<sub>3</sub> drops close to  
483 zero in Bode, Paknajol and Pulchowk in the winter season. This is a typical characteristic of  
484 many urban areas where reaction with NO at night depletes O<sub>3</sub> from the boundary layer (e.g.,  
485 Talbot et al., 2005). In the pre-monsoon and monsoon months, the titration is not as strong and  
486 the hourly O<sub>3</sub> falls, but generally remains above 10 ppb. Similar patterns of ozone mixing ratios  
487 were observed at other sites in northern South Asia. For example, higher O<sub>3</sub> mixing ratios were  
488 observed in the afternoon (84 ppb) and lower during the night and early morning hours (10 ppb)  
489 at Kullu Valley, a semi-urban site located at 1154 m asl, in the North-western Himalaya in India  
490 (Sharma et al. 2012). A similar dip in O<sub>3</sub> value in the dark hours was observed at Ahmedabad,  
491 India by Lal et al. (2000). Nagarkot, in contrast, is above the valley's boundary layer and has  
492 lesser NO for titration at night at this hill station as has been observed in another hill station in  
493 Himalayan foothills (Naja and Lal, 2002). Thus, the O<sub>3</sub> level remains above 25 ppb during the  
494 entire year at Nagarkot. As also shown in Table 3, at all sites, the O<sub>3</sub> mixing ratios were highest  
495 in the pre-monsoon, but the timing of the lowest seasonal values varied across the sites: post-  
496 monsoon in Bode, winter in Paknajol and monsoon in Nagarkot. Such differences in minimum  
497 O<sub>3</sub> across the sites can be anticipated due to the locations of the sites (e.g., urban, semi-urban,  
498 rural and hilltop sites, with differing availabilities of O<sub>3</sub> precursors from different emission  
499 sources). The seasonal variations of O<sub>3</sub> observed at Bode in this study are consistent with Putero  
500 et al. (2015) and Pudasainee et al. (2006), who also observed O<sub>3</sub> maxima during the pre-  
501 monsoon, but O<sub>3</sub> minima during the winter season.

502 The daily maximum 8-hour average O<sub>3</sub> mixing ratio (solid colored circles in Figure 6) exceeded  
503 the WHO recommended guideline of 50 ppb (WHO, 2006, black dotted line in Figure 6) most  
504 frequently during the pre-monsoon period and the winter. During the observation period, the  
505 daily maximum 8-hour average O<sub>3</sub> exceeded the WHO guideline on 102 out of 353 days of  
506 observation (29%) at Bode, 132/354 days (37%) at Paknajol and 159/357 days (45%) at  
507 Nagarkot. The higher exceedance rate at Nagarkot is because it is at higher altitude, which  
508 results in (i) greater exposure to large-scale regional pollution, especially from forest fire in the  
509 Himalayan foothills and agro-residue burning in the IGP region, outside the Kathmandu Valley  
510 (Sinha et al., 2014, Putero et al., 2015), (ii) less titration of O<sub>3</sub> by NO<sub>x</sub>, being farther away from  
511 the main pollution sources, and (iii) exposure to O<sub>3</sub> rich free tropospheric air, including  
512 influences from stratospheric intrusions. The diurnal profiles of O<sub>3</sub> mixing ratios (Figure 7) at

513 three sites Bode and Pakanajol in the Valley and Nagarkot, a hilltop site normally above the  
514 Kathmandu Valley's boundary layer shows, notably in the morning hours, that the residual layer  
515 above the Kathmandu Valley's mixing layer contains a significant amount of ozone. Based on  
516 the surface ozone data collected at Paknajok during 2013-14, Putero et al. (2015) concluded that  
517 downward mixing of ozone from the residual layer contributes to surface ozone in the  
518 Kathmandu Valley in the afternoon hours (11:00-17:00 local time). It is likely that the same  
519 source has also contributed to higher ozone mixing ratios at Nagarkot. Such mixing has been  
520 observed at other sites as well. Wang et al. (2012) reported the increase in downward mixing of  
521 O<sub>3</sub> from the stratosphere to the middle troposphere (56%) and the lower troposphere (13%) in  
522 spring and summer in Beijing. The downward flux was highest in the middle troposphere (75%)  
523 in winter. Similarly, Kumar et al. (2010) reported that more than 10 ppb of stratospheric  
524 contribution at a high altitude site (in Nainital) during January to April. However, there were no  
525 significant stratospheric intrusions seen in spring and summer (seen only in winter) at Nepal  
526 Climate Observatory-Pyramid (Putero et al., 2016).

527 During the SusKat-ABC campaign in 2013 and later in 2014, passive sampling of gaseous  
528 pollutants (SO<sub>2</sub>, NO<sub>x</sub>, NH<sub>3</sub> and O<sub>3</sub>) was carried out at fourteen sites including urban/semi-urban  
529 sites (Bode, Indrachowk, Maharajganj, Mangal Bazar, Suryabinayak, Bhaisepati,  
530 Budhanilkantha, Kirtipur, and Lubhu) and rural sites (Bhimdhunga, Naikhandi, Sankhu,  
531 Tinpiple, and Nagarkot) in the Kathmandu Valley (Kiros et al., 2016). Similar to this study, they  
532 also observed higher O<sub>3</sub> mixing ratios in rural areas than the urban/semi-urban sites in the  
533 Kathmandu Valley. Exceedances of the WHO standard are most common during the pre-  
534 monsoon season, occurring 78% (72/92 days), 88% (78/89 days) and 92% (85/92 days) of the  
535 time at Bode, Paknajok and Nagarkot, respectively. A study by Putero et al., (2015), based on O<sub>3</sub>  
536 mixing ratio measurements at Paknajok in the Kathmandu Valley, as a part of the SusKat-ABC  
537 campaign, has reported that the dynamics (both by horizontal and vertical winds) plays a key role  
538 in increased O<sub>3</sub> mixing ratios in the afternoon in the Kathmandu Valley. They estimated that the  
539 contribution of photochemistry varied as a function of the hour of the day, ranging from 6 to 34  
540 %. Unfortunately, no viable NO<sub>x</sub> measurements were obtained at any site in the Kathmandu  
541 Valley and surrounding mountain ridges during the SusKat-ABC campaign. Speciated VOCs  
542 were measured at Bode only for about 2 months but NO<sub>x</sub> was not available for the same period.  
543 Therefore we were not able to discern quantitatively proportional contributions of NO<sub>x</sub>, VOCs

544 and intrusion (chemistry vs. dynamics) from the free troposphere or lower stratosphere to  
545 observed O<sub>3</sub> concentrations at Nagarkot, Bode and other sites in the Valley. In the context of  
546 protecting public health, crops and regional vegetation, the O<sub>3</sub> mixing ratios in the Kathmandu  
547 Valley and surrounding areas clearly indicate the urgent need for mitigation action aimed at  
548 reducing emissions of its precursor gases NO<sub>x</sub> and VOCs. However, air quality management  
549 plans need to consider carefully the reduction strategies of NMVOCs or NO<sub>x</sub> while aiming at  
550 mitigating the O<sub>3</sub> pollution in the Kathmandu Valley. If the correct strategy (NMVOCs vs. NO<sub>x</sub>)  
551 is not applied, then O<sub>3</sub> mixing ratios could increase, for example, as seen in Huszar et al. (2016)  
552 where they reported that reducing NMVOCs in urban areas in central Europe leads to O<sub>3</sub>  
553 reduction whereas the focus on NO<sub>x</sub> reduction results in O<sub>3</sub> increase.

554  
555 The SusKat-ABC O<sub>3</sub> data can be compared to observations made about a decade ago by  
556 Pudasainee et al. (2006) at the urban site of Pulchowk, not far from Paknajol, as plotted in Figure  
557 6d. The daily maximum 8-hour average O<sub>3</sub> had exceeded the WHO guideline at Pulchowk for  
558 33% (95/292 days) of days during the observation from November 2003 to October 2004. The  
559 exceedance was 38% (133/354 days) of days at Paknajol during Feb 2013 - March 2014. Due to  
560 inter-annual variability and differences in the seasonal observation time periods at Pulchowk and  
561 Pakanajol, we cannot draw any conclusions about trends over the decade between the  
562 observations because of the difference in location and sampling height as well as a general  
563 difference in instrument calibration. However, a clear similarity between the observations is that  
564 most of the exceedance took place during pre-monsoon season, during which both studies have  
565 observations throughout the season (~90 days). The percentage of exceedance at Pulchowk  
566 during the pre-monsoon season in 2003-2004 was 70% (63/90 days) and at Pakanajol in 2013 it  
567 was 88% (78/89 days). However, just like for the annual fraction of exceedances, due to inter-  
568 annual variability we cannot say that the 18% (or ca. 15 days) difference in the exceedances is  
569 significant. A longer term O<sub>3</sub> record would be needed to really establish if there is a trend in the  
570 ozone concentrations.

571

### 572 **3.4 O<sub>3</sub> seasonal and diurnal variation**

573 The seasonal average O<sub>3</sub> mixing ratios at Bode, Nagarkot and Paknajol are shown in Table 3. For  
574 comparison, the O<sub>3</sub> mixing ratios measured at two sites in India, (i) Manora Peak (1958 m asl),

575 ca. 9 km from Nainital city, a site in rural mountain setting and (ii) Delhi, a highly-polluted  
576 urban setting in northwest IGP are also listed in the Table, based on results from Kumar et al.  
577 (2010) and Ghude et al. (2008). There is a strong similarity between the urban and semi-urban  
578 sites in Nepal (i.e., Bode, Pakanajol) and India (i.e., Delhi), as well as between the rural and  
579 mountain sites in Nepal (i.e., Nagarkot) and India (i.e., Manora Peak), with small differences.  
580 The peak mixing ratios were in the pre-monsoon period: at the rural and mountain sites the peak  
581 ozone mixing ratio values were very similar (64 and 62 ppb for Nagarkot and Manora Peak,  
582 respectively) and are due to influences discussed earlier for Nagarkot; at the sub-urban and urban  
583 sites the pre-monsoon values are significantly lower (ca. 40, 42, 33 ppb for Bode, Paknajok,  
584 Delhi, respectively) due to fresh NO<sub>x</sub> emissions near the urban sites and the consequent titration  
585 of ozone with NO. The lowest O<sub>3</sub> seasonal values at rural and mountain sites typically occur in  
586 the monsoon months while for semi-urban and urban sites, the minimum was observed during  
587 post-monsoon (Bode) and winter (Paknajok).

588 Figure 7 shows the diurnal variation of O<sub>3</sub> mixing ratios at Bode, Paknajok and Nagarkot in the  
589 different seasons. The typical O<sub>3</sub> maximum mixing ratio in the early afternoon at the urban and  
590 semi-urban sites is mainly due to daytime photochemical production as well as entrainment of  
591 ozone due to dynamics (both intrusion of ozone rich free tropospheric air into the boundary  
592 layer, and regional scale horizontal transport of ozone), as explained in case of Paknajok by  
593 Putero et al. (2015).

594 The ozone mixing ratios are relatively constant throughout the day at Nagarkot (~1901 m asl),  
595 which, being a hilltop site, is largely representative of the lower free tropospheric regional  
596 pollution values, however, it is also affected by ozone production from precursors transported  
597 from the Kathmandu Valley due to westerly winds during the afternoon hours. The dip in O<sub>3</sub> at  
598 Nagarkot (Figure 7) in the morning transition hours indicates the upward mixing of air from  
599 polluted (and Ozone-depleted) nocturnal boundary layer as it is breaking up.

### 600 **3.5 CO emission flux estimate**

601 It is possible to determine a top-down estimate of the average CO emission flux for the morning  
602 hours for the region around the Bode site by applying an approach that was developed and used  
603 in Mues et al. (2017) to estimate the emission fluxes of BC at Bode. The analysis of Mues et al.  
604 (2017) found BC fluxes for the Kathmandu Valley that were considerably higher than the

605 widely-used EDGAR HTAP emission database (Version 2.2). Support for this top-down estimate  
 606 was found by considering the BC concentrations and fluxes for the Kathmandu Valley in  
 607 comparison to Delhi and Mumbai; although the observed BC concentrations were similar in all  
 608 three locations, the EDGAR HTAP V2.2 emissions of BC for the Kathmandu Valley are much  
 609 lower than those for Delhi and Mumbai, while the top-down emissions estimate for the  
 610 Kathmandu Valley were similar to the emissions from EDGAR HTAP V2.2 for Delhi and  
 611 Mumbai (Mues et al., 2017).

612  
 613 Here we apply the same method as developed in Mues et al. (2017) to estimate the CO fluxes  
 614 based on the observed CO mixing ratio and ceilometer observations of the mixing layer height  
 615 (*MLH*) in Bode for the period of 1 year (March 2013-February 2014). Using the approach used  
 616 by Mues et al. (2017), the CO fluxes can be calculated from the increase in CO concentrations  
 617 during the nighttime period when the *MLH* is nearly constant, using:

$$618 \quad FCO(t_x, t_y) = \frac{\Delta CO \times ave(MLH(t_x), MLH(t_y))}{\Delta t \times 3600} \times \frac{MLH(t_y)}{MLH(t_x)} \quad (1)$$

619  
 620 where  $FCO(t_x, t_y)$  is the CO emission flux (in  $\mu\text{g m}^{-2} \text{s}^{-1}$ ) between time  $t_x$  and  $t_y$  (in hours),  $\Delta CO$   
 621 is the change in CO mixing ratio (in  $\mu\text{g m}^{-3}$ ) between time  $t_x$  and  $t_y$ ,  $ave(MLH(t_x), MLH(t_y))$  are  
 622 average of the mixing layer heights (in m) between time  $t_x$  and  $t_y$ ,  $\Delta t$  is the time interval between  
 623  $t_x$  and  $t_y$ , and  $MLH(t_y)/MLH(t_x)$  is mixing layer collapse factor, accounting for the small change in  
 624 *MLH* between the night and the morning hours. The calculation of the emission flux is based on  
 625 mean diurnal cycle per month of CO and *MLH* and  $t_x$  and  $t_y$  represent the time with the  
 626 minimum ( $t_x$ ) and the maximum ( $t_y$ ) CO concentration in the night and morning (see Mues et al.,  
 627 2017 for details).

628  
 629 This method of calculating the CO emission flux is based on five main assumptions: (i) CO is  
 630 well-mixed horizontally and vertically within the mixing layer in the region immediately  
 631 surrounding the Bode site; (ii) the *MLH* remains fairly constant during the night so that the  
 632 product of the CO concentration ( $\mu\text{g m}^{-3}$ ) and the *MLH* (m) represents CO mass per unit area  
 633 within the column, and any change in mass per unit area represents the net flux into the column;

634 (iii) the transport of air pollutants into and out of the stable nocturnal boundary layer of the  
635 valley is negligible, which is supported by the calm winds ( $<1 \text{ m s}^{-1}$ ) during the night and  
636 morning hours at the site (Mahata et al., 2017), (iv) the vertical mixing of pollutants between the  
637 mixing layer and the free atmosphere is assumed to be negligible at night, thus strictly seen is the  
638 estimated CO flux calculated with eq. 1 only valid for the morning hours. When applied to the  
639 whole day the implicit assumption is that the emissions are similar during the rest of the 24 h  
640 period. An assumption that is viable on average for some sources like brick kilns which operate  
641 day and night, but which does not apply to all sources, e.g., the technique will tend to  
642 underestimate emissions due to traffic, which are typically much stronger during the day than at  
643 night, while it will overestimate emissions due to waste burning, which is typically more  
644 prevalent during the night and early morning (pre-sunrise) than during the daytime. Assumption  
645 (iv) is made because equation 1 only works well for calculating the CO flux at night-morning  
646 period, when there is a relatively constant *MLH* and limited vertical and horizontal mixing; and  
647 v) CO emission is assumed to be uniform throughout the valley; this may not be correct, but  
648 cannot be verified until a high resolution emission inventory data is available, which is being  
649 developed for the Kathmandu Valley and rest of Nepal with a 1 km x 1km spatial resolution  
650 (Sadavarte et. al., 2018). During nighttime assumption (i) might not be entirely correct since the  
651 degree of mixing in the nocturnal stable layer and thus the vertically mixing is drastically  
652 reduced compared to daytime (and thus the term “mixing layer” is not entirely accurate, but we  
653 nevertheless apply it here due to its common use with ceilometer measurements). This adds a  
654 degree of uncertainty to the application of ceilometer observations to compute top-down  
655 emissions estimates, which will only be resolved once nocturnal vertical profile measurements  
656 are also available in order to characterize the nocturnal boundary layer characteristics and the  
657 degree to which the surface observations are representative of the mixing ratios throughout the  
658 vertical column of the nocturnal stable layer.

659 It is not possible to directly compute the emission flux for a full 24-hour day using this top-down  
660 method, since the emissions during the day could be either greater or smaller than at night, and  
661 because the other assumptions do not hold (in particular there is considerable vertical mixing  
662 with the free troposphere and stronger horizontal transport during the daytime). Thus the top-  
663 down computation only provides a useful indicative value. However, while it is also not possible  
664 to estimate how much different the daytime emissions are, it is possible to determine an absolute

665 lower bound for the CO flux ( $FCO_{min}$ ) by making the extreme assumption that the CO emissions  
666 are non-zero only during the hours which were used in the calculation, and that they were zero  
667 during the rest of the day (this provides a lower bound to the emissions since the daytime  
668 emissions physically cannot be negative). This lower bound of the flux ( $FCO_{min}$ ) is thus  
669 calculated by scaling back the 24-hour flux to only applying over the calculation time interval  
670 ( $\Delta t$ ), using:

$$FCO_{min.} = FCO \times \frac{\Delta t}{24} \quad (2)$$

672  
673 Figure 8 shows the estimated monthly CO emission flux, along with its 25<sup>th</sup> and 75<sup>th</sup> percentile  
674 values as an indication of the variability of the estimated flux in each month; the lower bound of  
675 the CO flux based on Equation 2 is also shown. The estimated annual mean CO flux at Bode is  
676  $4.9 \mu\text{g m}^{-2} \text{s}^{-1}$ . Seasonally, the emissions are computed to be highest during December to April  
677 ( $3.6\text{-}8.4 \mu\text{g m}^{-2} \text{s}^{-1}$ ), coinciding with the brick kiln operation period, which resulted in elevated  
678 concentrations of most pollutants at Bode (Kim et al., 2015; Chen et al., 2016; Sarkar et al.,  
679 2016; Mahata et al., 2017; Mues et al., 2017), including CO (Bhardwaj et al., 2017; Mahata et  
680 al., 2017), while the emissions were generally lower during the remaining months ( $0.5\text{-}5.4 \mu\text{g m}^{-2}$   
681  $\text{s}^{-1}$ ). The uncertainty in the top-down CO emissions estimate will be largest during June to  
682 October, due to the greater diurnal and day-to-day variability with the minimum and maximum  
683 CO mixing ratio values during the night and early morning used in Equation 1 often being less  
684 distinct than in the other months.

685  
686 Comparing the annual mean top-down estimated CO emission flux at Bode ( $4.9 \mu\text{g m}^{-2} \text{s}^{-1}$ ) with  
687 available global and regional emission inventories, the top-down estimated CO flux is twice the  
688 value,  $2.4 \mu\text{g m}^{-2} \text{s}^{-1}$ , for the Kathmandu Valley in the EDGAR HTAP V2.2 emission inventory  
689 database for 2010 [note that the CO emission values for the location at Bode and the whole  
690 averaged for the valley ( $27.65\text{-}27.75^\circ\text{N}$ ,  $85.25\text{-}85.40^\circ\text{E}$ ) were found to be the same up to two  
691 significant figures]. The estimated CO flux was 6.5-8 times as high as in the REAS database  
692 ( $0.63\text{-}0.76 \mu\text{g m}^{-2} \text{s}^{-1}$ , based on the 2008 values in Kurokawa et al., 2013), and between 3 and 14  
693 times higher than the values in the INTEX-B database for 2006 ( $0.35\text{-}1.77 \mu\text{g m}^{-2} \text{s}^{-1}$ ; Zhang et

694 al., 2009). The large differences between our estimated CO emission flux and these emission  
695 databases is not likely to be due to the comparison of data for different years; rather, it indicates  
696 the substantial uncertainties in both the top-down and bottom-up approaches to estimating the  
697 emission flux. Although our approximation of the emission flux relies on several assumptions,  
698 the fact that the lower bound value that we calculate is still as high as or higher than the values in  
699 some of the published emission datasets likely indicates that the bottom-up emissions are  
700 missing or underestimating some important sources, which will be important to examine  
701 carefully and improve as a basis for interpreting future modelling studies of CO pollution in the  
702 Kathmandu Valley and surrounding regions, as well as for assessing possible mitigation options.

703  
704 The emission estimates computed here are subject to several further uncertainties which are  
705 discussed in detail in Mues et al., (2017). In short, the uncertainties of CO flux estimates arise  
706 from (i) the assumptions that Bode site represents the whole atmospheric column and entire  
707 valley, which is not possible to verify without having many simultaneous monitoring stations in  
708 the valley (measurements at a few sites where CO was monitored for this study show some  
709 difference in CO mixing ratios), (ii) the higher variability (unclear minima and maxima during  
710 the morning and night hours) in the diurnal cycles of CO from June to October show a much  
711 higher variability than other months, that in turn makes it difficult to choose the exact hour of  
712 CO minimum and maximum needed for the flux estimation and (iii) the possible impact of wet  
713 deposition is not taken into account but would rather cause to generally underestimate the  
714 emission rate.

#### 715 **4. Conclusions**

716 Ambient CO and O<sub>3</sub> mixing ratios were measured in the framework of the SusKat-ABC  
717 international air pollution measurement campaign at five sites (Bode, Paknajol, Bhimdhunga,  
718 Naikhandi and Nagarkot) in the Kathmandu Valley (Table 1) and its fringes, initially during  
719 January to July 2013, and later extended to one year at three sites (Bode, Paknajol and Nagarkot)  
720 to better understand their seasonal characteristics. The observed CO and O<sub>3</sub> levels at all sites  
721 except Nagarkot were characteristic of highly-polluted urban settings, with the particular feature  
722 that the bowl-shaped valley and resulting meteorology had several effects on the pollution levels.

723 At all sites, the CO mixing ratios were higher during the early morning and late evening,  
724 especially an observation connected to the interplay between the ventilation of the boundary  
725 layer and the diurnal cycles of the emission sources. Under calm wind conditions that limited  
726 mixing within, into and out of the Kathmandu Valley, the morning CO peak tended to be more  
727 pronounced due to the buildup of pollution at night in the shallow planetary boundary layer. This  
728 nocturnal buildup was especially strong during January to April at Bode, with the mean CO  
729 mixing ratio increasing by about a factor of 4 in the 12 hours from 20:00 to 08:00, especially due  
730 to operation of nearby brick kilns continuing through night. During the daytime, the wind  
731 becomes stronger and the horizontal and vertical circulation dilutes and transports pollution  
732 around and out of the valley. Although normally the pollution levels are presumed to be higher in  
733 the heavily populated valley than in the immediate surrounding region, occasionally the synoptic  
734 circulation will transport in CO and O<sub>3</sub>-rich air, especially influenced by forest fires and agro-  
735 residue burning in the IGP region and Himalayan foothills, as was observed on a few episodes in  
736 the pre-monsoon season.

737 The observed O<sub>3</sub> mixing ratio was highest in the pre-monsoon season at all sites, and the daily  
738 maximum 8-hour average O<sub>3</sub> exceeded the WHO guideline of 50 ppb on about 80% of the days  
739 during this season at the semi-urban/urban sites of Bode and Paknajol, while at Nagarkot (which  
740 is in the free troposphere, i.e., above valley's boundary layer most of the time, especially during  
741 nighttime) it exceeded the WHO guideline on 92% of the days in pre-monsoon season. During  
742 the whole observation period, the 8 hour maximum average O<sub>3</sub> exceeded the WHO  
743 recommended value on 29%, 37% and 45% of the days at Bode, Paknajol and Nagarkot,  
744 respectively. The diurnal cycle showed evidence of photochemical production, larger scale  
745 advection of polluted air masses as well as possible down-mixing of O<sub>3</sub> during the daytime, as  
746 also observed by Putero et al., (2015) at Paknajol, with the hourly mixing ratio at the polluted  
747 site increasing from typically 5-20 ppb in the morning to an early afternoon peak of 60-120 ppb  
748 (Putero et al., 2015; Bhardwaj et al., 2018).

749 These high O<sub>3</sub> levels have deleterious effects on human health and ecosystems, including agro-  
750 ecosystems in the Kathmandu Valley and surrounding regions, thus justifying mitigation  
751 measures to help reduce the levels of O<sub>3</sub> (its precursors VOCs and NO<sub>x</sub>), CO and other  
752 pollutants. Determining the most effective mitigation measures will be challenging due to the

753 complicated interplay of pollution and meteorology as well as local and regional pollution  
754 sources. This study has provided information on current ambient levels and the diurnal/seasonal  
755 variations. This will be helpful in the design of future policies, both as a baseline for evaluating  
756 the effectiveness of mitigation measures, as well as giving insight into the connections between  
757 various pollutant sources (e.g., brick kilns) and their impacts on seasonally elevated CO levels,  
758 especially at nighttime. One particular contribution has been the development of a top-down  
759 estimate of the total emission flux of CO at Bode, which was found to be  $4.9 \mu\text{g m}^{-2} \text{s}^{-1}$ . This is  
760 several times higher (by a factor of 2-14 times) than the CO emission fluxes for the Kathmandu  
761 Valley in state-of-the-art inventories such as EDGAR-HTAP, REAS, and INTEX-B. This points  
762 out the need for the development of updated comprehensive emission inventory databases for  
763 this region. The improved emission inventory is necessary to provide more accurate input to model  
764 simulations to assess air pollution processes and mitigation options for the Kathmandu Valley  
765 and the broader surrounding region.

766 While the high levels of particulate pollution in the Kathmandu Valley have caught the main  
767 attention of the public and policymakers, due to their immediately visible nature, our paper  
768 points out that ozone is also a serious problem here. In fact, its higher levels on the nearby  
769 mountaintop location of Nagarkot, which is much more representative of regional air pollution,  
770 point to an ozone problem in the wider foothills of the Himalayas. In fact the extent of ozone  
771 pollution in the large surrounding Himalayan foothills has been insufficiently recognized until  
772 our study. This needs monitoring and research to identify feasible mitigation options.

773

#### 774 **Data Availability**

775 The observational data collected for this study will be made public through the SusKat website  
776 of IASS. They are also available upon direct request sent to [maheswar.rupakheti@iass-](mailto:maheswar.rupakheti@iass-potsdam.de)  
777 [potsdam.de](mailto:maheswar.rupakheti@iass-potsdam.de) and [khadak.mahata@iass-potsdam.de](mailto:khadak.mahata@iass-potsdam.de).

778

#### 779 **Acknowledgement**

780 We are thankful to the funders of the IASS – the German Ministry of Education and Research  
781 (BMBF) and the Brandenburg State Ministry of Science, Research and Culture (MWFK) – for

782 their generous support in making these measurements and their analysis possible. This study was  
783 partially supported by core funds of ICIMOD contributed by the governments of Afghanistan,  
784 Australia, Austria, Bangladesh, Bhutan, China, India, Myanmar, Nepal, Norway, Pakistan,  
785 Switzerland, and the United Kingdom, as well as by funds from the Government of Sweden to  
786 ICIMOD's Atmosphere Initiative. The authors would like to thank Bhupesh Adhikary,  
787 Bhogendra Kathayat, Shyam Newar, Dipesh Rupakheti, Nirjala Koirala, Ashish Bhatta, Begam  
788 Roka, Sunil Babu Khattry, Giampietro Verza, and several staff members at the Kamdhenu  
789 Madhyamik Vidhyalaya, Naikhandi who assisted in the field measurements, Siva Praveen  
790 Puppala for initial data processing, and Pankaj Sadavarte for helping with the emission  
791 databases. We are grateful to the Department of Environmental Sciences, University of Virginia,  
792 USA, for making available CO and O<sub>3</sub> instruments for the measurements. We also thank the staff  
793 at Real Time Solutions (RTS), Lalitpur, Nepal for providing an automatic weather station.  
794

## 795 **References**

- 796 Avnery, S., Mauzerall, D. L., Liu, J., and Horowitz, L. W.: Global crop yield reductions due to  
797 surface ozone exposure: 1. Year 2000 crop production losses and economic damage, *Atmos.*  
798 *Environ.*, 45, 2284–2296, doi:10.1016/j.atmosenv.2010.11.045, 2011.
- 799  
800 Bhardwaj, P., Naja, M., Rupakheti, M., Panday, A. K., Kumar, R., Mahata, K., Lal, S.,  
801 Lawrence, M. G., Chandola, H. C.: Variations in surface ozone and CO in the Kathmandu Valley  
802 during SusKat-ABC international field campaign, *Atmos. Chem. Phys. Discuss.*,  
803 <https://doi.org/10.5194/acp-2017-306>, 2017.
- 804 Bonasoni P., P. Laj, A. Marinoni, M. Sprenger, F. Angelini, J. Arduini, U. Bonafè, F. Calzolari,  
805 T. Colombo, S. Decesari, C. Di Biagio, A. G. di Sarra, et. al.: Atmospheric brown clouds in the  
806 Himalayas: first two years of continuous observations at the Nepal Climate Observatory-Pyramid  
807 (5079 m). *Atmos. Chem. Phys.*, 10, 7515-7531, 2010.
- 808 Brauer, M., Amman, M., Burnett, R. T., Cohen, A., Dentener, F., Zenati, M., Henderson, S. B.,  
809 Krzyzanowski, M., Martin, R. V., Van Dingenen, R., van Donkelaar, A., and Thurston, G. D.:

810 Exposure assessment for estimation of the global burden of disease attributable to outdoor air  
811 pollution, *Environ. Sci. Technol.*, 46, 652–660, doi:10.1021/es2025752, 2012.

812 Burney, J., and Ramanathan, V.: Recent climate and air pollution impacts on Indian agriculture,  
813 *Proceedings of the National Academy of Sciences of the United States of America*, 111, 16319-  
814 16324, doi:10.1073/pnas.1317275111, 2014.

815 Chen, P., Kang, S., Li, C., Rupakheti, M., Yan, F., Li, Q., Ji, Z., Zhang, Q., Luo, W., Sillanpää,  
816 M.: Characteristics and sources of polycyclic aromatic hydrocarbons in atmospheric aerosols in  
817 the Kathmandu Valley, Nepal, *Sci. Total Environ.*, 538, 86-92, doi:  
818 10.1016/j.scitotenv.2015.08.006, 2015.

819 Cristofanelli, P., Bracci, A., Sprenger, M., Marinoni, A., Bonafè, U., Calzolari, F., Duchi, R.,  
820 Laj, P., Pichon, J. M., Roccato, F., Venzac, H., Vuillermoz, E., and Bonasoni, P.: Tropospheric  
821 ozone variations at the Nepal Climate Observatory- Pyramid (Himalayas, 5079ma.s.l.) and  
822 influence of deep stratospheric intrusion events, *Atmos. Chem. Phys.*, 10, 6537–6549,  
823 doi:10.5194/acp-10-6537-2010, 2010.

824 Dentener, F., Stevenson, D., Ellingsen, K., Van Noije, T., Schultz, M., Amann, M., Atherton, C.,  
825 Bell, N., Bergmann, D., and Bey, I.: The global atmospheric environment for the next  
826 generation, *Environ. Sci. Technol.*, 40, 3586-3594, 2006.

827 Davidson, C. I., Lin, S.-F., and Osborn, J. F.: Indoor and outdoor air pollution in the Himalayas,  
828 *Environ. Sci. Technol.*, 20(6), 561 – 566, doi:10.1021/es00148a003, 1986.

829 Dhungel, S., Kathayat, B., Mahata, K., and Panday, A.: Transport of regional pollutants through  
830 a remote trans-Himalayan valley in Nepal, *Atmos. Chem. Phys.*, 18, 1203-1216,  
831 <https://doi.org/10.5194/acp-18-1203-2018>, 2018.

832 Department of Transport Management (DoTM): Annual report of Ministry of Labor and  
833 Transport Management, Government of Nepal, 2015.

834 Forouzanfar, M. H., Alexander, L., Anderson, H. R., Bachman, V. F., Biryukov, S., Brauer, M.,  
835 Burnett, R., Casey, D., Coates, M. M., and Cohen, A.: Global, regional, and national comparative  
836 risk assessment of 79 behavioural, environmental and occupational, and metabolic risks or

837 clusters of risks in 188 countries, 1990–2013: a systematic analysis for the global burden of  
838 disease study 2013, *Lancet*, 386, 2287-2323, doi: 10.1016/S0140-6736(15)00128-2, 2015.

839 Fowler, D., Flechard, C., Cape, J. N., Storeton-West, R. L., and Coyle, M.: Measurements of  
840 ozone deposition to vegetation quantifying the flux, the stomatal and nonstomatal components,  
841 *Water Air Soil Pollut.*, 130, 63–74, doi:10.1023/a:1012243317471, 2001.

842 Fueglistaler, S., Dessler, A. E., Dunkerton, T. J., Folkins, I., Fu, Q., and Mote, P. W.: Tropical  
843 tropopause layer, *Rev. Geophys.*, 47, RG1004, doi:10.1029/2008RG000267, 2009.

844 Geiß, A., Wiegner, M., Bonn, B., Schäfer, K., Forkel, R., von Schneidmesser, E., Munkel, C.,  
845 Chan, K. L., and Nothard, R.: Mixing layer height as an indicator for urban air quality?, *Atmos.*  
846 *Meas. Tech. Discuss.*, 2017, 1-32, doi:10.5194/amt-2017-53, 2017.

847 Giri, D., Murthy, K., Adhikary, P., Khanal, S.: Ambient air quality of Kathmandu Valley as  
848 reflected by atmospheric particulate matter concentrations (PM10), *Int. J. Environ. Sci. Technol.*  
849 3, 403–410, 2006.

850 Highwood, E. J. and Hoskins, B. J.: The tropical tropopause, *Q. J. Roy. Meteorol. Soc.*, 124,  
851 1579–1604, doi:10.1002/qj.49712454911, 1998.

852 Huszar, P., Belda, M., and Halenka, T.: On the long-term impact of emissions from central  
853 European cities on regional air quality, *Atmos. Chem. Phys.*, 16, 1331–1352, doi:10.5194/acp-  
854 16-1331-2016, 2016.

855 International Energy Agency (IEA): Energy and air pollution, *World Energy Outlook Special*  
856 *Report 2016*, International Energy Agency, 2016.

857 Janssens-Maenhout, G., Dentener, F., van Aardenne, J., Monni, S., Pagliari, V., Orlandini, L.,  
858 Klimont, Z., Kurokawa, J., Akimoto, H., Ohara, T., Wankmüller, R., Battye, B., Grano, D.,  
859 Zuber, A., and Keating, T.: EDGAR-HTAP: a harmonized gridded air pollution emission dataset  
860 based on national inventories, *Tech. Rep. JRC68434*, Publications Office of the European Union,  
861 doi:10.2788/14102 (online), <http://publications.jrc.ec.europa.eu/repository/handle/JRC68434>,  
862 2000.

863 Kiros, F., Shakya, K. M., Rupakheti, M., Regmi, R. P., Maharjan, R., Byanju, R. M., Naja, M.,  
864 Mahata, K., Kathayat, B., and Peltier, R. E.: Variability of Anthropogenic Gases: Nitrogen  
865 oxides, sulfur dioxide, ozone and ammonia in Kathmandu Valley, Nepal, *Aerosol Air Qual. Res.*,  
866 16: 3088–3101, 2016.

867 Kumar, R., Naja, M., Venkataramani, S., and Wild, O.: Variation in surface ozone at Nainital: A  
868 high-altitude site in the central Himalayas, *J. Geophys. Res.*, 115 (D16),  
869 doi:10.1029/2009JD013715, 2010.

870 Kurokawa, J., Ohara, T., Morikawa, T., Hanayama, S., Janssens-Maenhout, G., Fukui, T.,  
871 Kawashima, K., and Akimoto, H.: Emissions of air pollutants and greenhouse gases over Asian  
872 regions during 2000-2008: Regional emission inventory in Asia (REAS) version 2, *Atmos.*  
873 *Chem. Phys.*, 13, 11 019–11 058, doi:10.5194/acp-13-11019-2013, 2013.

874 Lal, S., Naja, M., and Subbaraya B. H.: Seasonal variations in surface ozone and its precursors  
875 over an urban site in India, *Atmos. Environ.*, 34, 2713-2724, doi: 10.1016/S1352-  
876 2310(99)00510-5, 2000.

877 Lawrence, M., and Lelieveld, J.: Atmospheric pollutant outflow from southern Asia: a review,  
878 *Atmos. Chem. Phys.*, 10, 11017-11096, 2010.

879 Lim, S. S., Vos, T., Flaxman, A. D., Danaei, G., Shibuya, K., Adair-Rohani, H., Amann, M.,  
880 Anderson, H. R., Andrews, K. G., Aryee, M., Atkinson, C., Bacchus, L. J., Bahalim, A. N.,  
881 Balakrishnan, K., Balmes, J., Barker-Collo, S., Baxter, A., Bell, M. L., Blore, J. D., Blyth, F.,  
882 Bonner, C., Borges, G., Bourne, R...and Ezzati, M.: A comparative risk assessment of burden of  
883 disease and injury attributable to 67 risk factors and risk factor clusters in 21 regions, 1990-2010:  
884 a systematic analysis for the global burden of disease study 2010, *Lancet*, 380, 2224–2260, 2012.

885 Lüthi, Z. L., Škerlak, B., Kim, S. W., Lauer, A., Mues, A., Rupakheti, M., and Kang, S.:  
886 Atmospheric brown clouds reach the Tibetan Plateau by crossing the Himalayas, *Atmos. Chem.*  
887 *Phys.* 15, 6007-6021, doi:10.5194/acp-15-6007-2015, 2015.

888 Mahata, K. S., Panday, A. K., Rupakheti, M., Singh, A., Naja, M., and Lawrence, M. G.:  
889 Seasonal and diurnal variations of methane and carbon dioxide in the Kathmandu Valley in the

890 foothills of the central Himalaya, *Atmos. Chem. Phys. Discuss.*, 2017, 1-55, doi:10.5194/acp-  
891 2016-1136, 2017.

892 Marinoni, A., Cristofanelli, P., Laj, P., Duchi., R., Putero, D., Calzolari, F., Landi., T. C.,  
893 Vuillermoz, E., Maione, M., and Bonasoni, P.: High black carbon and ozone concentrations  
894 during pollution transport in the Himalayas: Five years of continuous observations at NCO-P  
895 global GAW station, *J. Environ. Sci.*, 25(8) 1618–1625, 2013.

896 Ming, J., Xiao, C., Sun, J., Kang, S.-C, and Bonasoni, P.: Carbonaceous particles in the  
897 atmosphere and precipitation of the Nam Co region, central Tibet, *J. Environ. Sci.-CHINA*,  
898 22(11), 1748-1756, 2010.

899 Monks, P. S., Granier, C., Fuzzi, S., Stohl, A., Williams, M. L., Akimoto, H., Amann, M.,  
900 Baklanov, A., Baltensperger, U., Bey, I., Blake, N., Blake, R. S., Carslaw, K., Cooper, O. R.,  
901 Dentener, F., Fowler, D., Fragkou, E., Frost, G. J., Generoso, S., Ginoux, P., Grewe, V.,  
902 Guenther, A., Hansson, H. C., Henne, S., Hjorth, J., Hofzumahaus, A., Huntrieser, H., Isaksen, I.  
903 S. A., Jenkin, M. E., Kaiser, J., Kanakidou, M., Klimont, Z., Kulmala, M., Laj, P., Lawrence, M.  
904 G., Lee, J. D., Liousse, C., Maione, M., McFiggans, G., Metzger, A., Mieville, A.,  
905 Moussiopoulos, N., Orlando, J. J., O’Dowd, C. D., Palmer, P. I., Parrish, D. D., Petzold, A.,  
906 Platt, U., Poeschl, U., Prevot, A. S. H., Reeves, C. E., Reimann, S., Rudich, Y., Sellegri, K.,  
907 Steinbrecher, R., Simpson, D., ten Brink, H., Theloke, J., van derWerf, G. R., Vautard, R.,  
908 Vestreng, V., Vlachokostas, C., and von Glasow, R.: Atmospheric composition change – global  
909 and regional air quality, *Atmos. Environ.*, 43, 5268–5350, doi:10.1016/j.atmosenv.2009.08.021,  
910 2009.

911 Mues, A., Rupakheti, M., Münkkel, C., Lauer, A., Bozem, H., Hoor, P., Butler, T., and Lawrence,  
912 M.: Investigation of the mixing layer height derived from ceilometer measurements in the  
913 Kathmandu Valley and implications for local air quality, *Atmos. Chem. Phys.*, doi:10.5194/acp-  
914 17-8157, 2017.

915 Naja, M., and Lal, S.: Surface ozone and precursor gases at Gadanki (13.5°N, 79.2°E), a tropical  
916 rural site in India, *J. Geophys. Res.* 107 (D14), ACH 8-1-ACH 8–13, doi:10.1029/2001jd000357,  
917 2002.

918 Nayava, J. L.: Rainfall in Nepal, the Himalayan Rev. Nepal, Geographical Society, 12:1– 18,  
919 1980.

920 Organisation for Economic Co-operation and Development (OECD): The economic  
921 consequences of outdoor air pollution, OECD Publishing,  
922 doi: <http://dx.doi.org/10.1787/9789264257474-en>, 2016.

923 Panday, A. K., and Prinn, R. G.: Diurnal cycle of air pollution in the Kathmandu Valley, Nepal:  
924 Observations, *J. Geophys. Res.*, 114 (D9), doi:10.1029/2008JD009777, 2009.

925 Panday, A. K. Prinn, R. G., and Schär, C.: Diurnal cycle of air pollution in the Kathmandu  
926 Valley, Nepal: 2. Modeling results, *J. Geophys. Res.*, 114 (D21), doi:10.1029/2008JD009808,  
927 2009.

928 Pudasainee, D., Sapkota, B., Shrestha, M. L., Kaga, A., Kondo, A., and Inoue, Y.: Ground level  
929 ozone concentrations and its association with NO<sub>x</sub> and meteorological parameters in Kathmandu  
930 Valley, Nepal, *Atmos. Environ.*, 40(40), 8081–8087, doi:10.1016/j.atmosenv.2006.07.011, 2006.

931 Putero, D., Cristofanelli, P., Marinoni, A., Adhikary, B., Duchi, R., Shrestha, S.D., Verza, G.P.,  
932 Landi, T.C., Calzolari, F., Busetto, M., Agrillo, G., Biancofiore, F., Di Carlo, P., Panday, A. K.,  
933 Rupakheti, M., and Bonasoni, P.: Seasonal variation of ozone and black carbon observed at  
934 Paknajol, an urban site in the Kathmandu Valley, Nepal. *Atmos. Chem. Phys.*, 15(24), 13957-  
935 13971, doi:10.5194/acp-15-13957-2015, 2015.

936 Putero, D., Cristofanelli, P., Sprenger, M., Škerlak, B., Tositti, L., and Bonasoni, P.: STEFLUX,  
937 a tool for investigating stratospheric intrusions: application to two WMO/GAW global stations.  
938 *Atmos. Chem. Phys.*, 16, 14203–14217, doi:10.5194/acp-16-14203-2016, 2016.

939 Ram, K., and Sarin, M.: Spatio-temporal variability in atmospheric abundances of EC, OC and  
940 WSOC over Northern India, *J. Aerosol Sci.*, 41, 88–98, 2010.

941 Regmi, R. P., Kitada, T., and Kurata, G.: Numerical simulation of late wintertime local flows in  
942 Kathmandu Valley, Nepal: Implication for air pollution transport, *J. Appl. Meteorol.*, 42, 389-  
943 403, 2003.

944 Rupakheti, M., Panday, A. K., Lawrence, M. G., Kim, S. W., Sinha, V., Kang, S. C., Naja, M.,  
945 Park, J. S., Hoor, P., Holben, B., Sharma, R. K., Mues, A., Mahata, K. S., Bhardwaj, P., Sarkar,  
946 C., Rupakheti, D., Regmi, R. P., and Gustafsson, Ö.: Air pollution in the Himalayan foothills:  
947 overview of the SusKat-ABC international air pollution measurement campaign in Nepal,  
948 *Atmos. Chem. Phys. Discuss.*, in preparation, 2017.

949 Rupakheti, D., Adhikary, B., Praveen, P. S., Rupakheti, M., Kang, S.-C., Mahata, K. S., Naja,  
950 M., Zhang, Q., Panday, A. K., and Lawrence, M. G.: Pre-monsoon air quality over Lumbini, a  
951 world heritage site along the Himalayan foothills, *Atmos. Chem. Phys.*, 17, 11041-111063,  
952 <https://doi.org/10.5194/acp-17-11041-2017>, 2017.

953 Sadavarte, P., Rupakheti, M., Shakya, K., Bhave, P.V., and Lawrence, M.G.: Nepal emission  
954 (NEEM): A high resolution technology - based bottom-up emissions inventory for Nepal, ACP  
955 in preparation, 2018.

956 Sarkar, C., Sinha, V., Kumar, V., Rupakheti, M., Panday, A., Mahata, K.S., Rupakheti, D.,  
957 Kathayat, B., and Lawrence, M.G.: Overview of VOC emissions and chemistry from PTR-TOF-  
958 MS measurements during the SusKat-ABC campaign: high acetaldehyde, isoprene and isocyanic  
959 acid in wintertime air of the Kathmandu Valley, *Atmos. Chem. Phys.*, 16, 3979-4003, 2016.

960 Sarkar, C., Sinha, V., Sinha, B., Panday, A. K., Rupakheti, M., and Lawrence, M. G.: Source  
961 apportionment of NMVOCs in the Kathmandu Valley during the SusKat-ABC international field  
962 campaign using positive matrix factorization, *Atmos. Chem. Phys.*, 17, 8129-8156, 2017.

963 Shakya, K. M., Rupakheti, M., Shahi, A., Maskey, R., Pradhan, B., Panday, A., Puppala, S. P.,  
964 Lawrence, M., and Peltier, R. E.: Near-road sampling of PM<sub>2.5</sub>, BC, and fine-particle chemical  
965 components in Kathmandu Valley, Nepal, *Atmos. Chem. Phys.*, 17, 6503-6516,  
966 <https://doi.org/10.5194/acp-17-6503-2017>, 2017.

967 Sharma, P., Kuniyal, J. C., Chand, K., Guleria, R. P., Dhyani, P. P. and Chauhan, C.: Surface  
968 ozone concentration and its behavior with aerosols in the northwestern Himalaya, India. *Atmos.*  
969 *Environ.* 71, 44-53, doi:10.1016/12.042, 2013.

970 Shrestha, A. B., Wake, C. P., Mayewski, P. A., and Dibb, J.E.: Maximum Temperature Trends in  
971 the Himalaya and Its Vicinity: An Analysis Based on Temperature Records from Nepal for the  
972 Period 1971–94, *J. Climate*, 12, 2775-2786, 1999.

973 Shrestha, S. R., Kim Oanh, N. T., Xu, Q., Rupakheti, M., and Lawrence, M. G.: Analysis of the  
974 vehicle fleet in the Kathmandu Valley for estimation of environment and climate co-benefits of  
975 technology intrusions, *Atmos. Environ.*, 81, 579-590, 2013.

976 Silva, R. A., West, J. J., Zhang, Y., Anenberg, S. C., Lamarque, J.-F., Shindell, D. T., Collins,  
977 W. J., Dalsoren, S., Faluvegi, G., Folberth, G., Horowitz, L. W., Nagashima, T., Naik, V.,  
978 Rumbold, S., Skeie, R., Sudo, K., Takemura, T., Bergmann, D., Cameron-Smith, P., Cionni, I.,  
979 Doherty, R. M., Eyring, V., Josse, B., MacKenzie, I. A., Plummer, D., Righi, M., Stevenson, D.  
980 S., Strode, S., Szopa, S., and Zeng, G.: Global premature mortality due to anthropogenic outdoor  
981 air pollution and the contribution of past climate change, *Environ. Res. Lett.*, 8, 034005,  
982 doi:10.1088/1748-9326/8/3/034005, 2013.

983 Talbot, R., Mao, H., and Sive, B.: Diurnal characteristics of surface level O<sub>3</sub> and other important  
984 trace gases in New England, *J. Geophys. Res.*, 110 (D9), doi:10.1029/2004JD005449, 2005.

985 Tripathee, L., Kang, S.-C., Huang, J., Sharma, C., Sillanpaa, M., Guo, J., and Paudyal, R.:  
986 Concentrations of trace elements in wet deposition over the central Himalayas, Nepal, *Atmos.*  
987 *Environ.*, 95, 231–238, 2014

988 Sinha, V., Kumar, V., and Sarkar, C.: Chemical composition of pre-monsoon air in the Indo-  
989 Gangetic Plain measured using a new air quality facility and PTR-MS: high surface ozone and  
990 strong influence of biomass burning, *Atmos. Chem. Phys.*, 14, 5921-5941, doi:10.5194/acp-14-  
991 5921-2014, 2014.

992 Tissier, A.-S. and Legras, B.: Convective sources of trajectories traversing the tropical  
993 tropopause layer, *Atmos. Chem. Phys.*, 16, 3383–3398, doi:10.5194/acp-16-3383-2016, 2016.

994 Vadrevu, K., Ellicott, E., Giglio, L., Badarinath, K., Vermote, E., Justice, C., Lau, W.:  
995 Vegetation fires in the Himalayan region - aerosol load, black carbon emissions and smoke  
996 plume heights, *Atmos. Environ.*, 47, 241–251, 2012.

997 Wang, Y., Konopka, P., Liu, Y., Chen, H., Müller, R., Plöger, F., Riese, M., Cai, Z., and Lü, D.:  
998 Tropospheric ozone trend over Beijing from 2002–2010: Ozonesonde measurements and  
999 modeling analysis, *Atmos. Chem. Phys.*, 12, 8389–8399, doi:10.5194/acp-12-8389-2012, 2012.

1000 World Health Organization (WHO): WHO Air quality guidelines for particulate matter, ozone,  
1001 nitrogen dioxide and sulfur dioxide, Global update 2005, Summary of risk assessment, WHO  
1002 Press, Geneva, Switzerland, 2006.

1003 World Health Organization (WHO): 7 million premature deaths annually linked to air pollution,  
1004 2014 (<http://www.who.int/mediacentre/news/releases/2014/air-pollution/en/>).

1005 Zhang, Q., Streets, D., Carmichael, G., He, K., Huo, H., Kannari, A., Klimont, Z., Park, I.,  
1006 Reddy, S., Fu, J., Chen, D., Duan, L., Lei, Y., Wang, L., and Yao, Z.: Asian emissions in 2006  
1007 for the NASA INTEX-B mission, *Atmos. Chem. Phys.*, 9, 5131–5153, 2009.

1008

**Table 1.** Information on the sampling sites (of the SusKat-ABC campaign) used in this study with sampling carried out during 2013-2014 in the Kathmandu Valley. The altitude is in meter above mean sea level (m asl)

Site	General setting of site	Location, altitude (m asl)
Bode	Sub-urban, tallest building with scattered houses surrounded by agricultural fields	27.69°N, 85.40°E, 1345
Bhimdhunga	Rural. On the ridge, close to the pass separating the Kathmandu Valley from a valley of a tributary the Trishuli River to the west	27.73°N, 85.23°E, 1522
Paknajol	Urban, city-center, the tallest building in the neighborhood	27.72°N, 85.30°E, 1380
Naikhandi	Rural, at outlet of Bagmati River in Southwest corner of the Valley	27.60°N, 85.29°E, 1233
Nagarkot	Mountain rural. Mountain top site of the eastern valley rim, north facing towards the Kathmandu Valley	27.72°N , 85.52°E, 1901

**Table 2.** Details of the instruments deployed at different sites during the observation period during January 2013-March 2014 in the Kathmandu Valley.

Location	Instrument	Parameters	Inlet/sensor height (above ground)	Duration	Group
1. Bode	a. Horiba APMA-370	CO	20 m	1 Jan-7 Jun 2013	ARIES
	b. Teledyne 400E	O <sub>3</sub>	20 m	1 Jan-7 Jun 2013	ARIES
	c. Thermo Scientific 49i	O <sub>3</sub>	20 m	18 Jun-31 Dec 2013	IASS
	d. Picarro G2401	CO	20 m	6 Mar 2013-5 Mar 2014	ICIMOD
	e. Campbell AWS	T, RH, SR, WS, WD, RF	22 m	1 Jan-30 Mar 2013	IASS
	f. Davis AWS (Vantage Pro2)	T, RH, P, RF	21 m	30 May-Jul 2013	UVA
	g. Ceilometer (Vaisala CL31)	MLH	20 m	01 Mar 2013- 28 Feb 2014	JGUM
2. Bhimdhunga	a. Thermo Scientific 48i	CO	2 m	1 Jan-15 Jul 2013	UVA
	b. AWS Hobo Onset	T, RH, SR, WS, WD, P	5 m	1 Jan-30 Jun 2013	UVA
3. Naikhandi	a. Thermo Scientific 48i	CO	5 m	3 Jan- 6 Jun 2013	UVA
	b. 2B Tech. Model 205	O <sub>3</sub>	5 m	1 Feb-25 May 2013	UVA
	c. AWS Hobo Onset	T, RH, SR, WS, WD, P	2 m	3 Jan-25 Apr 2013	UVA
4. Nagarkot	a. Thermo Scientific 48i	CO	5 m	13 Feb-Apr 3 2013; 8 Jun-15 Jul 2013	UVA
	b. Thermo Scientific 49i	O <sub>3</sub>	5 m	9 Jan-30 Jun 2013	UVA
	c. Campbell AWS	T, RH, SR, WS, WD, RF	7 m		IASS
	d. AWS (Vaisala WXT 520)	T, RH, SR, WS, WD, RF, P	7 m	10 Feb-30 Jun 2013	RTS
5. Paknajol	a. Thermo Environmental (49i)	O <sub>3</sub>	25 m	1 Feb 2013-30 Jan 2014	EV-K2-CNR
	b. AWS (Vaisala WXT 425)	T, RH, SR, WS, WD, RF, P	25 m	1 Feb 2013-30 Jan 2014	EV-K2-CNR

Note: T - temperature, RH - relative humidity, SR- solar radiation, WS - wind speed, WD - wind direction, RF- rainfall, P – pressure and MLH – Mixing layer height; ARIES - Aryabhata Research Institute of Observational Sciences, India; ICIMOD - International Center for Integrated Mountain Development, Nepal; IASS - Institute for Advanced Sustainability Studies, Germany; UVA- University of Virginia, USA; JGUM – Johannes Gutenberg University Mainz, Germany; RTS - Real Time Solutions, Nepal; Ev-K2-CNR - Everest-Karakorum - Italian National Research Council, Italy.

**Table 3.** Summary of the monthly average ozone mixing ratios (ppb) [average (Avg), standard deviation (SD), minimum (Min.) and maximum (Max.)] at four sites\* in the Kathmandu Valley, Nepal during 2013-2014 and two sites (Manora Peak and Delhi) in India

Month	Bode	Paknajol	Nagarkot	Manora <sup>a</sup> Peak	Delhi <sup>b</sup>
	Avg ± SD [Min., Max.]	Avg ± SD [Min., Max.]	Avg ± SD [Min., Max.]	Avg ± SD	Avg [Min., Max.]
January	23.5 ± 19.9 [1.4, 87.1]	16.9 ± 18.3 [0.1, 71.7]*	46.7 ± 5.7 [36.4, 73.7]	37.3 ± 14.8	19.3 [10, 14.7]
February	25.6 ± 20.4 [1.2, 94.5]	24.2 ± 20.1 [1.6, 91.7]	47.5 ± 7.5 [28.2, 83.6]	43.8 ± 16.8	25.3 [10.9, 55.7]
March	37.4 ± 24.3 [1.2, 105.9]	37.7 ± 23.8 [1.6, 95.8]	62.4 ± 9.5 [40.5, 98.9]	56.6 ± 11.4	29.7 [13.8, 58]
April	43.4 ± 26.6 [1.4, 116.2]	46.7 ± 26.8 [1.0, 115.5]	71.5 ± 15.5 [40.1, 121.0]	63.1 ± 11.7	33 [13.7, 64.3]
May	38.5 ± 21.2 [2.0, 111.1]	42.8 ± 20.6 [6.7, 103.3]	59.0 ± 20.6 [15.0, 124.5]	67.2 ± 14.2	35.4 [19.8, 62]
June	27.8 ± 12.0 [1.7, 68.4]	27.5 ± 17.0 [0.6, 90.7]	34.2 ± 9.1 [4.6, 72.0]	44.0 ± 19.5	25.6 [12.8, 46.4]
July	21.1 ± 9.5 [1.7, 82.0]	20.5 ± 13.4 [2.0, 77.9]	25.9 ± 6.2 [11.1, 48.0]	30.3 ± 9.9	19.1 [9.4, 37.1]
August	20.3 ± 9.9 [2.0, 70.9]	20.1 ± 12.6 [0.8, 73.1]	28.3 ± 5.8 [15.5, 62.9]	24.9 ± 8.4	14.3 [9.7, 29.5]
September	23.3 ± 14.9 [0.5, 85.9]	24.9 ± 17.4 [0.4, 108.1]	34.8 ± 9.6 [16.1, 79.7]	32.0 ± 9.1	17.7 [7.7, 37.7]
October	19.4 ± 13.8 [0.1, 70.9]	22.6 ± 17.0 [0.6, 83.5]	35.2 ± 10.2 [18.0, 73.8]	42.4 ± 7.9	21.7 [9, 56.9]
November	18.6 ± 15.1 [0.3, 67.7]	22.4 ± 20.9 [0.1, 84.0]	40.1 ± 8.1 [25.6, 73.3]	43.9 ± 7.6	22.6 [9, 55.1]
December	21.7 ± 17.8 [1.0, 96.6]	19.5 ± 19.7 [0.1, 82.0]	43.8 ± 9.0 [24.8, 85.11]	41.6 ± 6.3	20.2 [9.1, 40.3]
Season:					
Winter	24.5 ± 20.1 [1.2, 94.5]	20.2 ± 19.6 [0.1, 91.7]	45.8 ± 7.8 [24.8, 85.1]	40.9	21.6 [9.1, 55.7]
Pre-monsoon	39.8 ± 24.2 [1.2, 116.2]	42.4 ± 24.0 [1.0, 115.5]	64.3 ± 16.7 [14.9, 124.5]	62.3	32.7 [13.7, 64.3]
Monsoon	22.7 ± 12.0 [0.5, 85.9]	23.2 ± 15.5 [0.4, 108.1]	30.8 ± 8.7 [4.6, 79.7]	32.8	19.2 [7.7, 46.4]
Post-monsoon	19.0 ± 14.5 [0.1, 70.9]	22.5 ± 18.9 [0.1, 84.0]	37.6 ± 9.5 [18.0, 73.8]	39.4	22.2 [9, 56.9]

<sup>a</sup> Kumar et al. (2010), <sup>b</sup> Ghude et al. (2008). \* O<sub>3</sub> data of Paknajol on January was of 2014.

**Table 4.** Average CO mixing ratio (ppb) at different time of the day (daytime - 12:00 – 16:00), and nighttime - 23:00 – 03:00) and the monthly average (total) at four sites in the Kathmandu Valley.

Sites	Winter (16 Jan-15 Feb)			Pre-monsoon (16 Mar-15 Apr)			Monsoon (16 Jun-15Jul)			Post-monsoon (16 Oct-15 Nov)		
	daytime	nighttime	Total	daytime	nighttime	total	Daytime	nighttime	total	daytime	nighttime	total
Bode	405.35	927.21	819.17	430.91	839.17	770.52	210.59	230.08	241.34	269.10	453.95	397.24
Bhimdhunga	324.62	354.23	374.27	374.64	479.37	471.33	196.61	202.85	198.40			
Naikhandi	280.97	356.14	380.40	382.71	425.17	449.83						
Nagarkot							141.68	158.78	160.41			

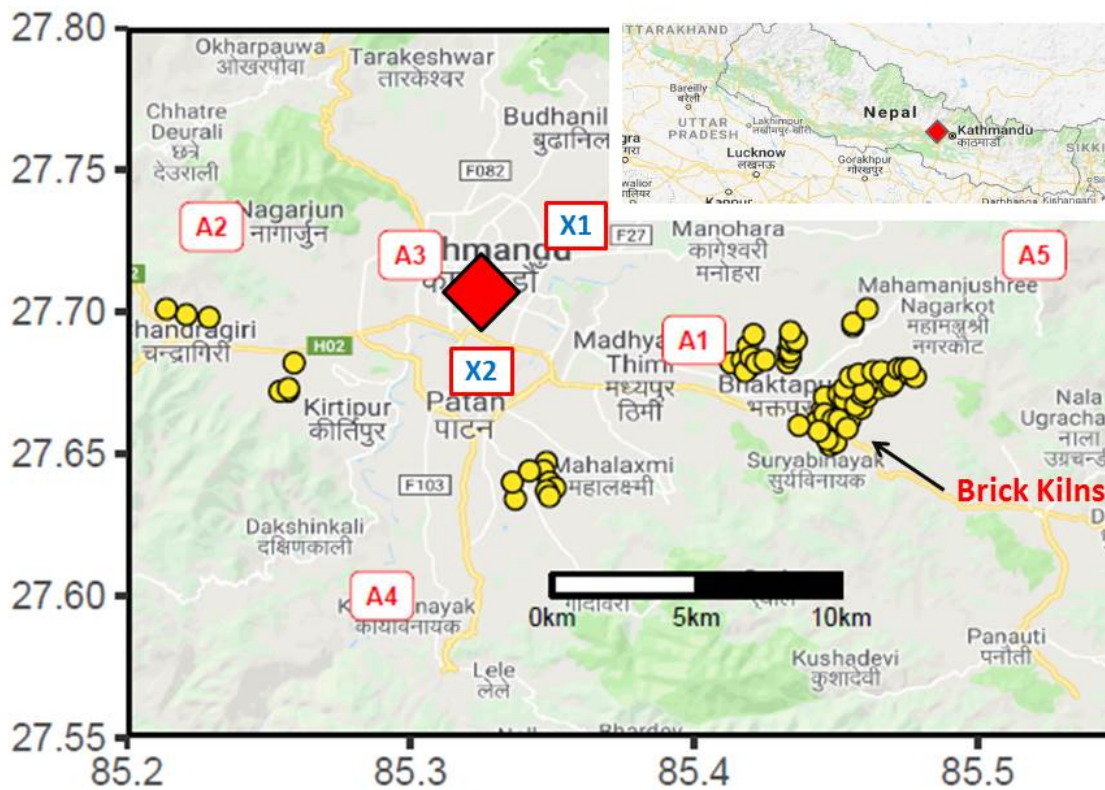


**Figure 1.** Observation sites in the SusKat-ABC international air pollution campaign during 2013-2014 in the Kathmandu Valley. A1 = Bode, A3 = Paknajol, and A4 = Naikhandi were selected within the valley floor and A2 = Bhimdhunga and A5 = Nagarkot on the mountain ridge. Naikhandi site is also near the Bagmati River outlet. Past study sites, Bouddha (X1) and Pulchowk (X2), which are referred in the manuscript, are also shown in the Figure. Source: Google Maps.

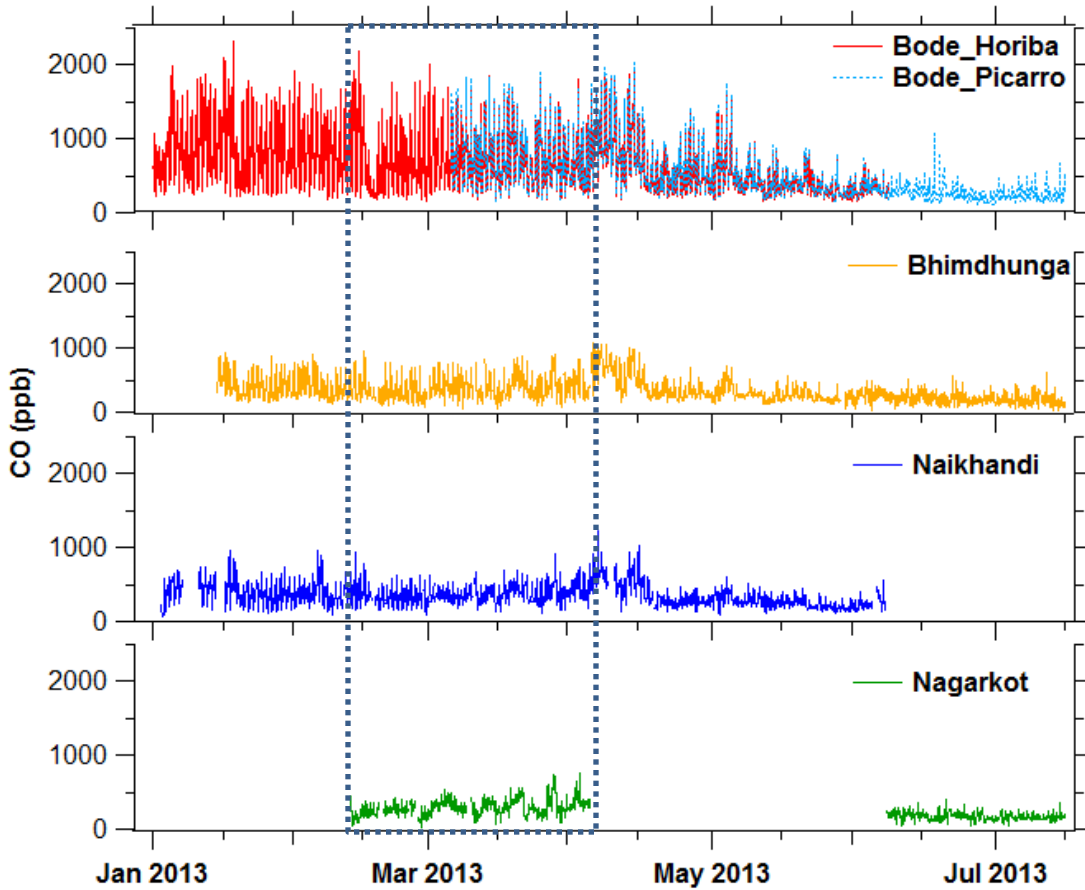


**Figure 2.** Hourly average CO mixing ratios observed at supersite (Bode) and three satellite sites (Bhimdhunga, Naikhandi and Nagarkot) of the SusKat-ABC international air pollution measurement campaign during January to July 2013 in the Kathmandu Valley. The dotted box represents a period (13 February - 03 April, 2013) during which data for all four sites were available.

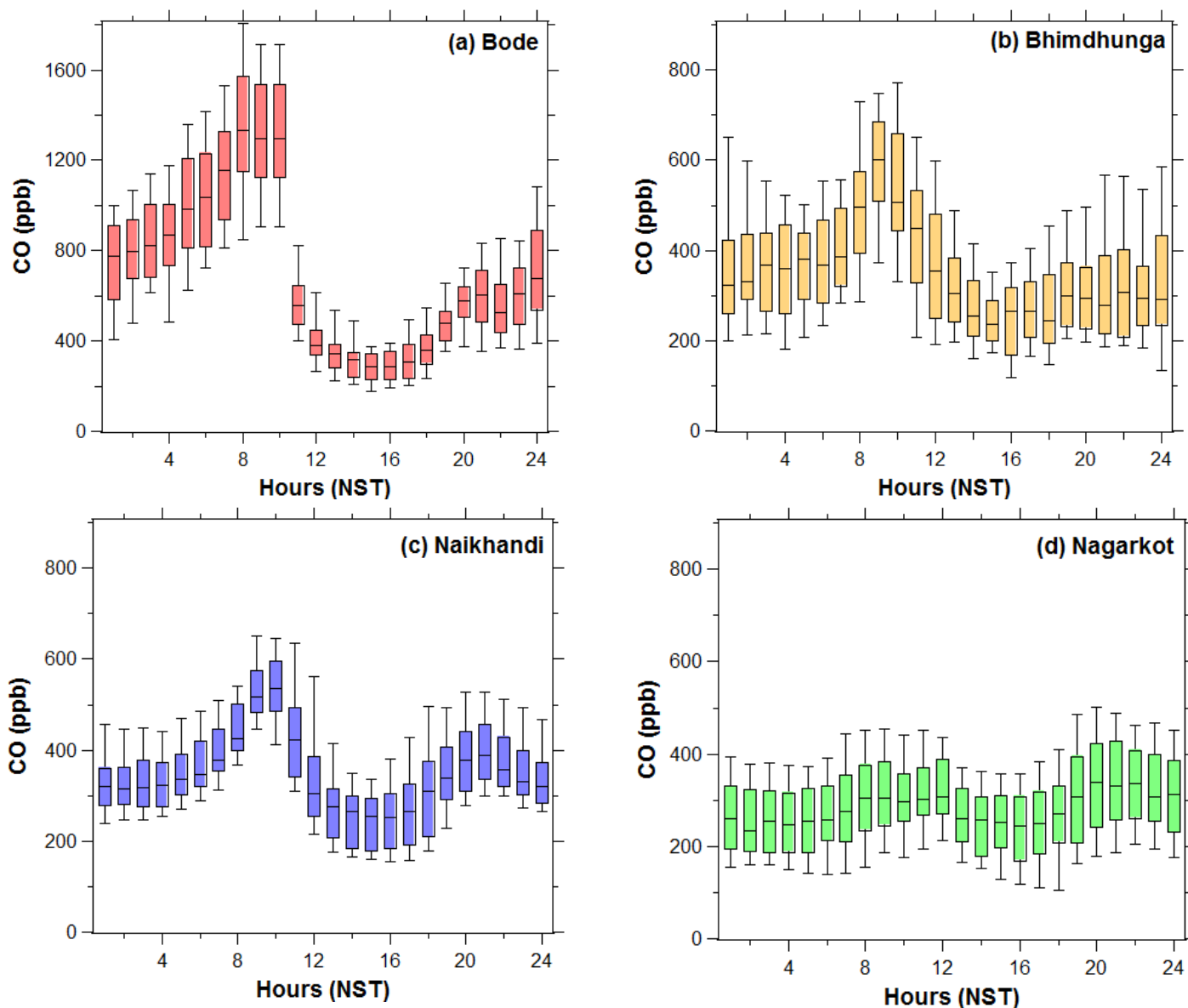


**Figure 3.** Diurnal variations of hourly average CO mixing ratios during the common observation period (13 February–03 April, 2013) at Bode, Bhimdhunga, Naikhandi and Nagarkot. The lower end and upper end of the whisker represents 10<sup>th</sup> and 90<sup>th</sup> percentile, respectively; the lower end and upper end of each box represents the 25<sup>th</sup> and 75<sup>th</sup> percentile, respectively, and the black horizontal line in the middle of each box is the median for each month. Note: the y-axis scale of Bode is twice that of the other three sites.

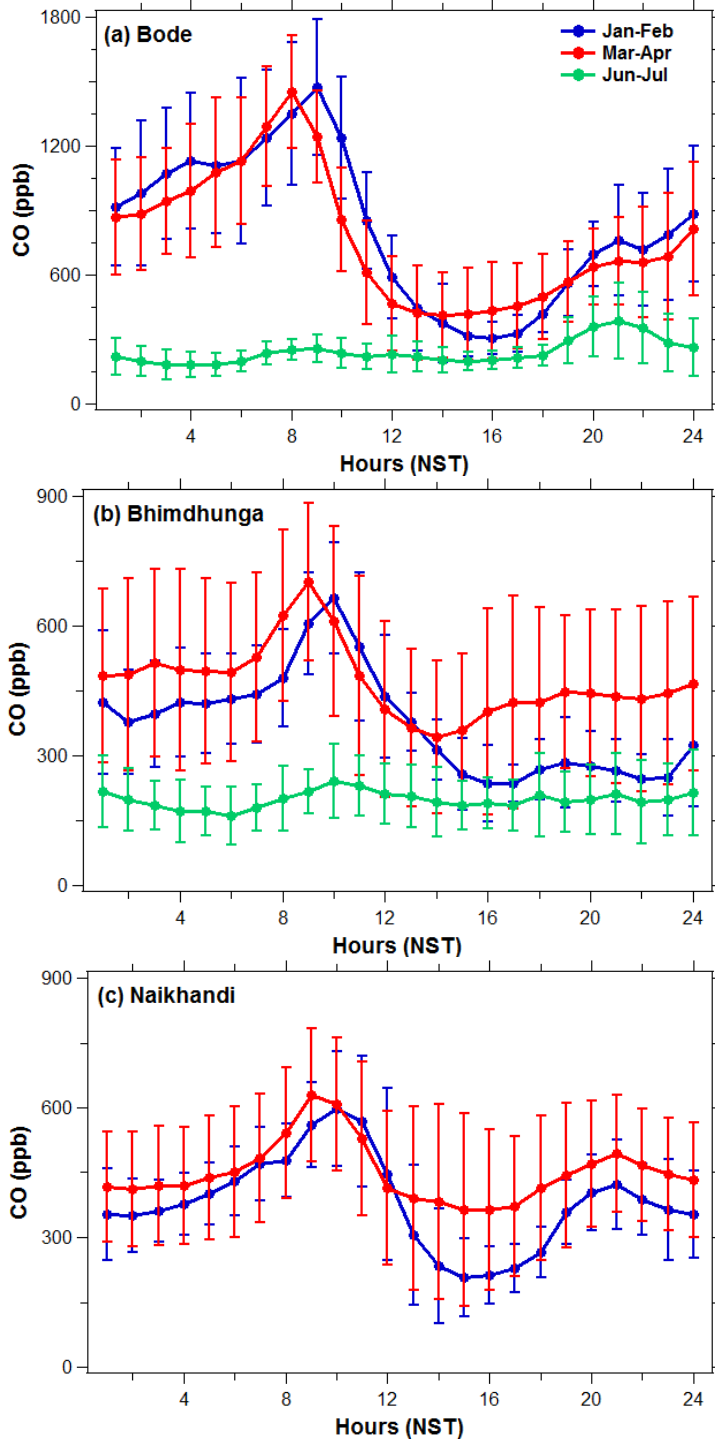


**Figure 4.** Comparison of diurnal variation of hourly average CO mixing ratios for four seasons at Bode, Bhimdhunga and Naikhandi. Due to the lack of continuous data at some sites, data of one month in each season were taken for comparison as representative of the winter (16 Jan – 15 Feb), pre-monsoon (16 Mar – 15 Apr) and monsoon (16 Jun – 15 Jul) season of 2013. Note: y-axis scale of the top panel (Bode) is double than lower two panels (Bhimdhunga and Naikhandi).

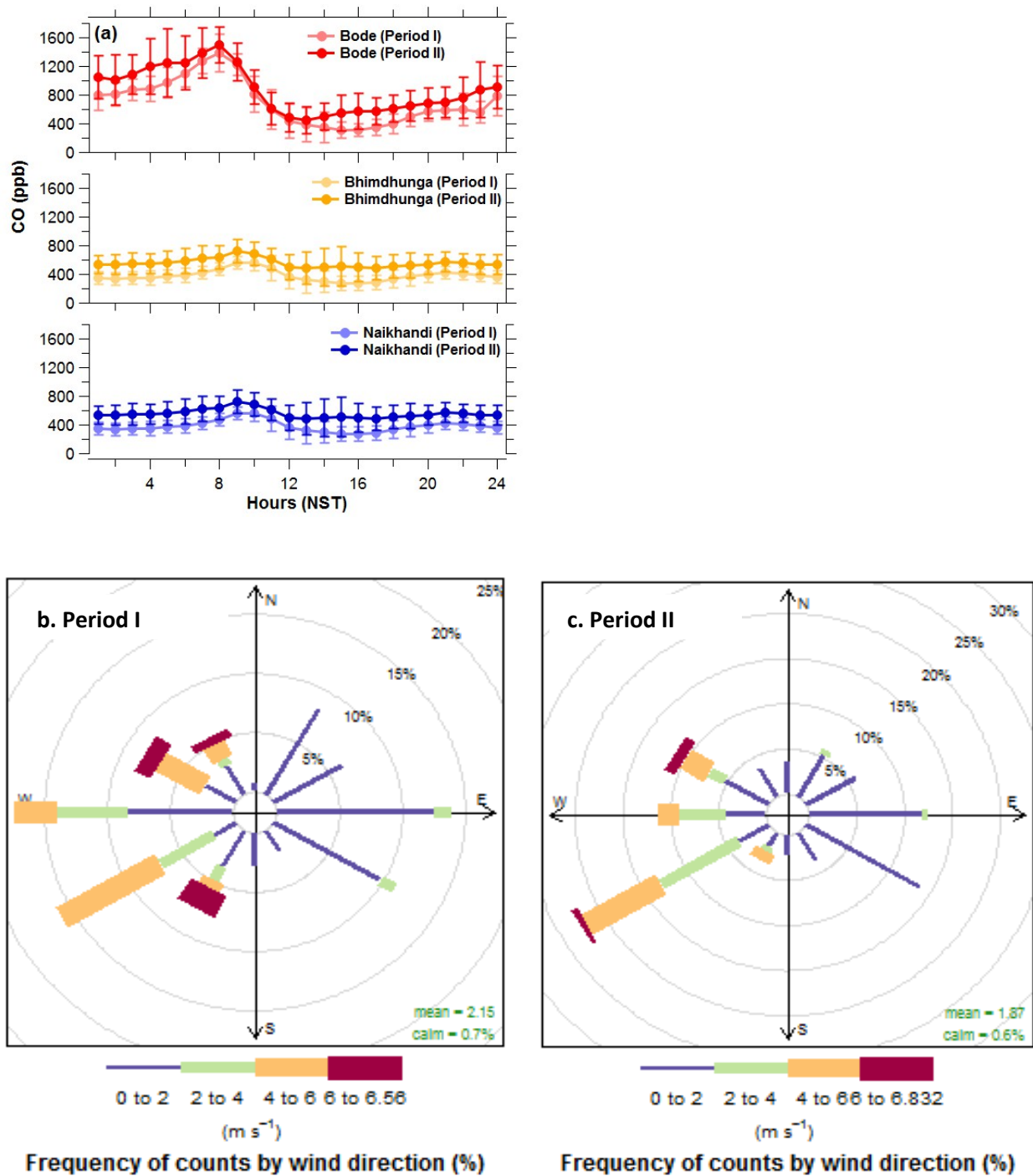


**Figure 5.** Comparison of hourly average CO mixing ratios during normal days (March 16-30), labelled as period I (faint color) and episode days (April 1-15), labelled as period II (dark color) in 2013 at (a) Bode, Bhimdhunga and Naikhandi in the Kathmandu Valley. The wind roses at Bode corresponding to two periods are also plotted (b) period I and (c) period II respectively.

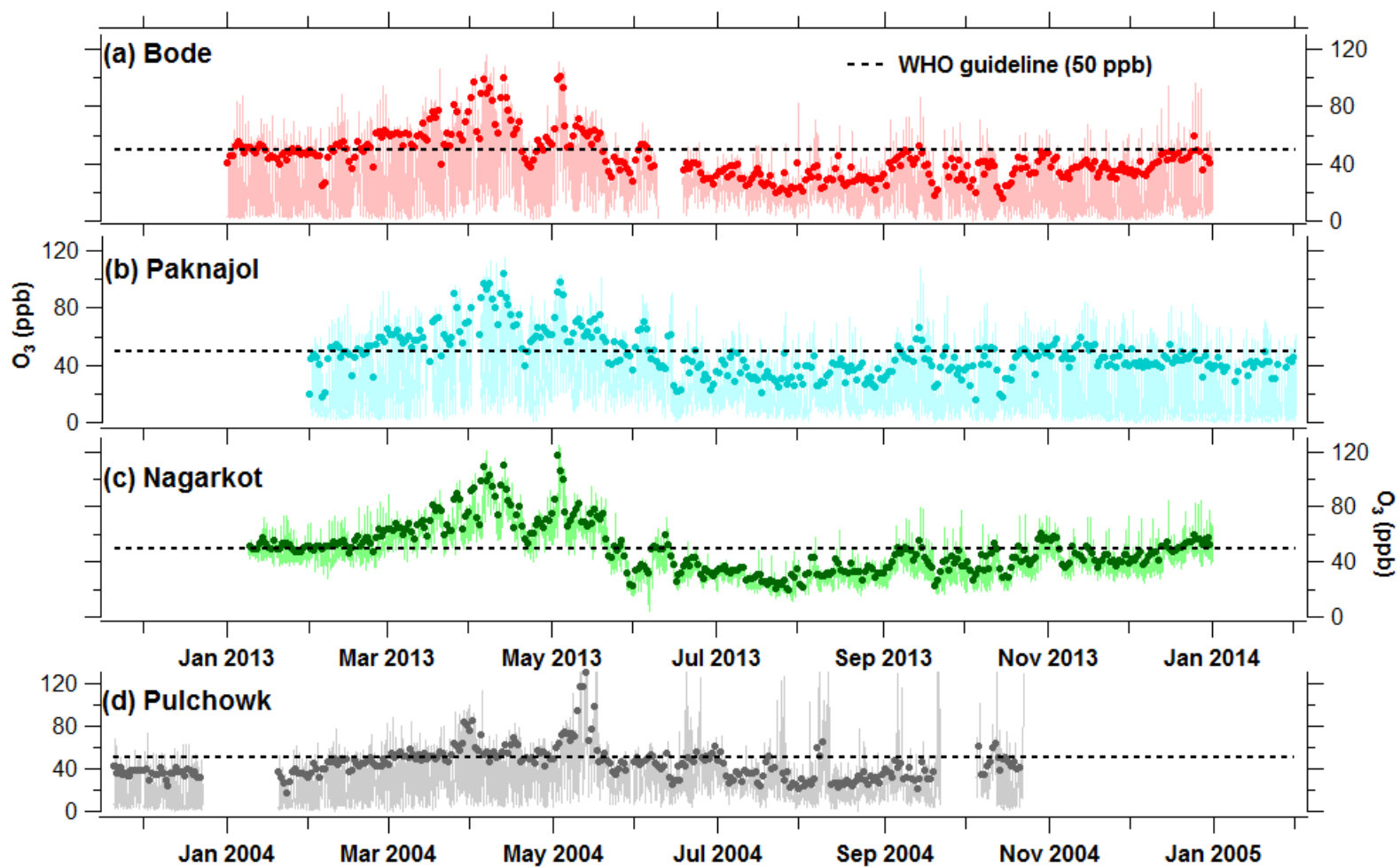


**Figure 6.** Time series of hourly average (faint colored line) and daily maximum 8-hr average (solid colored circle) O<sub>3</sub> mixing ratio at (a) Bode (semi-urban), (b) Paknajol (urban) and (c) Nagarkot (hilltop) observed during 2013-2014, and (d) Pulchowk (urban) observed during November 2003-October 2004 in the Kathmandu Valley. Black dotted line represents WHO guideline (50 ppb) for daily maximum 8-hour average of O<sub>3</sub>.

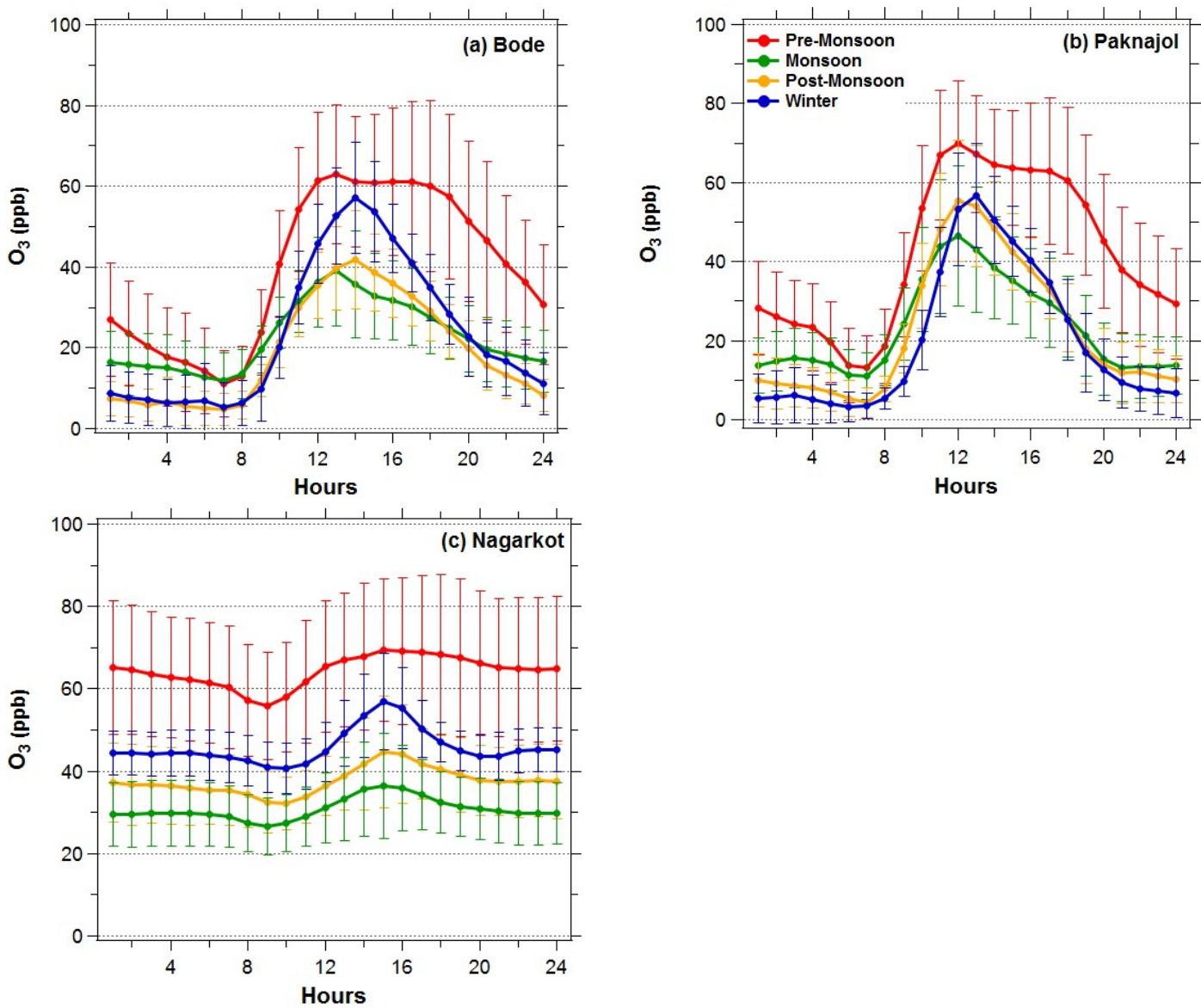


**Figure 7.** Diurnal pattern of hourly average  $O_3$  mixing ratio for different seasons during January 2013-January 2014 at (a) Bode, (b) Paknajol, and (c) Nagarkot in the Kathmandu Valley. The four seasons (described in the text) are defined as: pre-monsoon (Mar-May), monsoon (Jun-Sep), post-monsoon (Oct-Nov), winter (Dec-Feb).

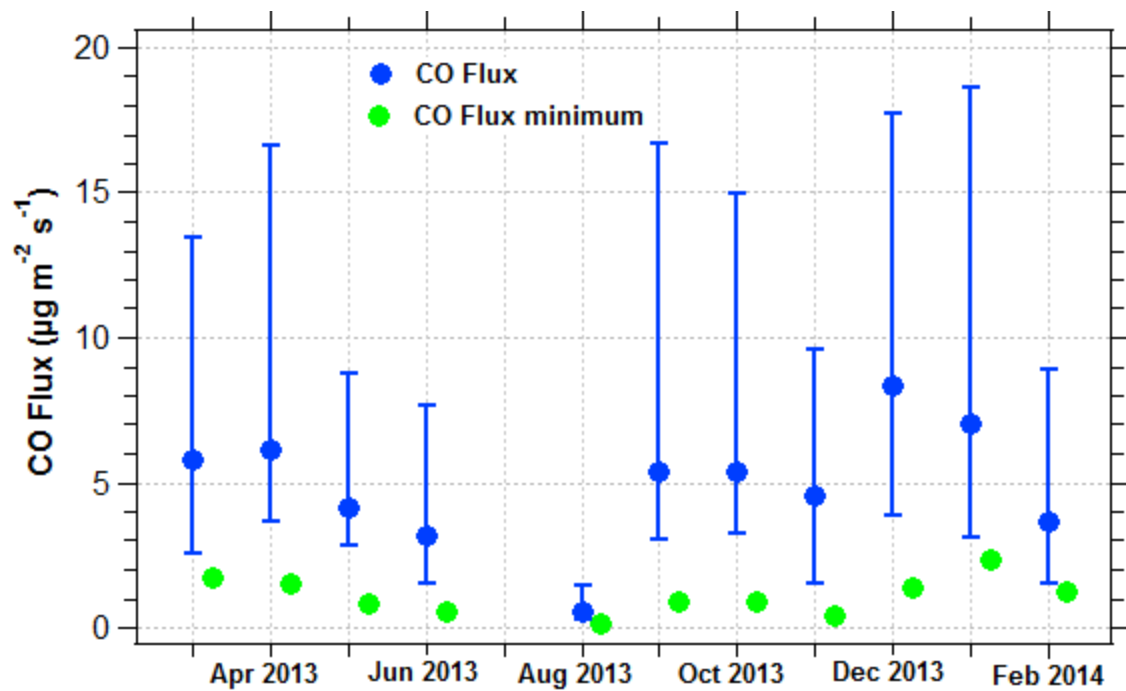


**Figure 8.** The estimated monthly average CO emission flux, which is based on the mean diurnal cycle of CO mixing ratios of each month for two conditions: (i) with data of all days (CO Flux) (blue dot) with lower and upper ends of the bar representing 25<sup>th</sup> and 75<sup>th</sup> percentile respectively, and (ii) with data of morning hours (CO Flux minimum) (green dot) in which zero emission is assumed for the other hours of the day. The fluxes for July were not estimated as there were insufficient (less than 15 days) of concurrent CO and mixing layer height data. It is expected that the  $F_{CO}$  and  $F_{CO_{min}}$  for July should fall between values for June and August 2013.